Progress in Oceanography 147 (2016) 49–66

Contents lists available at ScienceDirect

Progress in Oceanography

journal homepage: www.elsevier.com/locate/pocean

An inflated subpolar gyre blows life toward the northeastern Atlantic

H. Hátún [a,b,*], K. Lohmann [b], D. Matei [b], J.H. Jungclaus [b], S. Pacariz [a,c], M. Bersch [d], A. Gislason [e], J. Ólafsson [f], P.C. Reid [g,h,i]

[a] Faroe Marine Research Institute, Box 3051, FO-110 Tórshavn, Faroe Islands
[b] Max Planck Institute for Meteorology, Hamburg, Germany
[c] Department of Marine Sciences, University of Gothenburg, Gothenburg, Sweden
[d] University of Hamburg, Hamburg, Germany
[e] Marine Research Institute, 101 Reykjavik, Iceland
[f] Institute of Earth Sciences, University of Iceland, Reykjavik, Iceland
[g] Sir Alister Hardy Foundation for Ocean Science, Plymouth, UK
[h] Marine Institute, Plymouth University, Plymouth, UK
[i] Marine Biological Association of the UK, Plymouth, UK

ARTICLE INFO

Article history:
Received 14 April 2015
Received in revised form 26 May 2016
Accepted 15 July 2016
Available online 25 July 2016

ABSTRACT

Deep convection in the Labrador and Irminger Seas inflates the cold and low-saline subpolar gyre, which is a rich nutrient and zooplankton source for the surrounding warmer waters of subtropical origin. The zooplankton abundances on the south Iceland shelf show characteristic sub-decadal variability, which closely reflect the oceanic abundances of the ecologically most important zooplankton species – *Calanus finmarchicus*. Much higher abundances of this species are observed during years when the winter mixed layer depths (MLD) in the Labrador-Irminger Sea, and over the Reykjanes Ridge are deep. Furthermore, a tight relationship is identified between on-shelf zooplankton abundances and lateral shifts of the biologically productive subarctic front southwest of Iceland. Thus, we suggest that northeastward expansion of the subpolar gyre results in biologically productive periods in the waters southwest of Iceland – both oceanic and on the shelf. In addition to local atmospheric forcing, we find that the MLD and frontal position are also impacted by remote heat losses and convection in the Labrador Sea, through northward advection of unstable mode waters. The sub-decadal oceanic and on-shelf biological production peaks are possibly predictable by half a year (local winter convection to subsequent summer production), and the advective time-lag from the Labrador Sea might induce an even longer predictability horizon (up to 1.5 years).

1. Introduction

The North Atlantic Oscillation (NAO) is typically employed when attempting to associate ecosystem changes to climatic variability in the North Atlantic (Drinkwater et al., 2003; Greene and Pershing, 2000). Since many NAO-ecosystem links broke around the mid-1990s (Drinkwater et al., 2013; Hátún et al., 2007), there is a need to identify other physical metrics in addition to the NAO index. One such metric is the so-called gyre index, reflecting the strength and extent of the North Atlantic subpolar gyre (SPG) (Häkkinen and Rhines, 2004; Hátún et al., 2005). The SPG – a large body of cold and low-saline subarctic water, which circulates counterclockwise (Fig. 1) – declined after the mid-1990s (Häkkinen and Rhines, 2004). This resulted in a sudden warming and salinification in the subpolar North Atlantic due to increased northward intrusion of relatively warm and saline subtropical water from the eastern Atlantic (striped region in Fig. 1) (Bersch et al., 1999; Hátún et al., 2005; Robson et al., 2012). This water mixes with colder and fresher western water masses from the North Atlantic Current (NAC), producing SubPolar Mode Waters (SPMW, checkered region in Fig. 1) (McCartney and Talley, 1982) which flow and spread toward the Barents Sea in the north (Holliday et al., 2008) and the Labrador Sea in the west (McCartney and Talley, 1982). Fundamental ecosystem changes have been observed after this shift (Hátún et al., 2009a), and the gyre index has often been used as a physical metric for these changes (Hátún et al., 2009b; Hovland et al., 2013; Solmundsson et al., 2010). The NAO and the gyre indices co-varied before

* Corresponding author at: Havstovan, Nóatún 1, FO-110 Tórshavn, Faroe Islands.
E-mail addresses: hjalmarh@hav.fo (H. Hátún), katja.lohmann@mpimet.mpg.de (K. Lohmann), daniela.matei@mpimet.mpg.de (D. Matei), johann.jungclaus@mpimet.mpg.de (J.H. Jungclaus), selmap@hav.fo (S. Pacariz), manfred.bersch@zmaw.de (M. Bersch), assthor@hafro.is (A. Gislason), jo@hi.is, jon@hafro.is (J. Ólafsson), pcre@sahfos.ac.uk (P.C. Reid).

http://dx.doi.org/10.1016/j.pocean.2016.07.009
0079-6611/

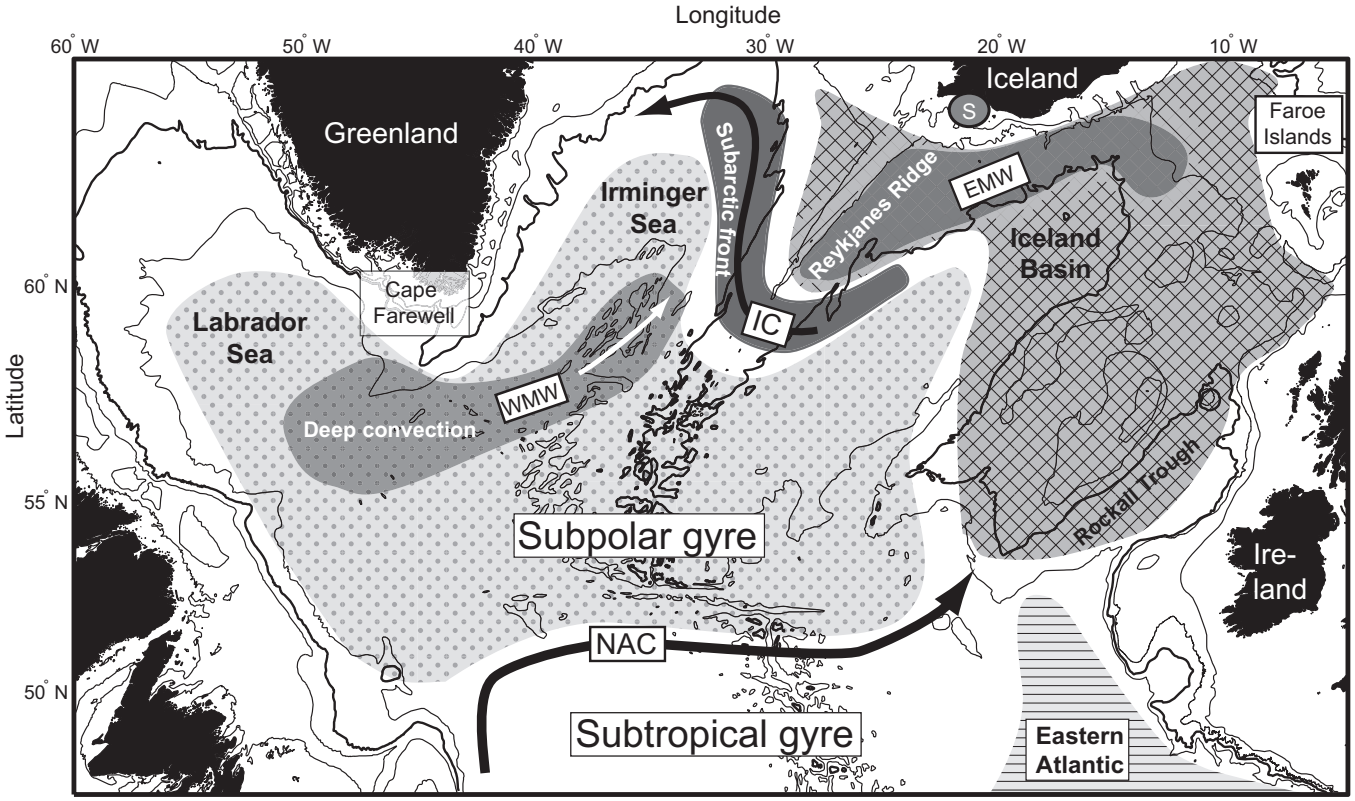

Fig. 1. Map of the subpolar North Atlantic Ocean. The subpolar gyre and the eastern source water area are shown with the dotted and striped regions, respectively, and the SPMW mixing region is illustrated with the checkered region. The core WMW (Western Mode Water) and EMW (Eastern Mode Water) regions, and the subarctic frontal zone, are shown with deeper gray shades. The currents - NAC (North Atlantic Current), IC (Irminger Current) – are outlined with the arrows. The 200 m, 1000 m, 2000 m (thick line) and 3000 m isobaths are shown, and the location of the on-shelf zooplankton measurement site is shown with the gray oval, marked with an 'S'.

1995, but while the NAO index switched to average values after a sudden dip during winter 1995–1996, the gyre index continued to decline (Häkkinen and Rhines, 2004; Hátún et al., 2005).

Strong surface heat losses over subpolar waters during the winter, represented by a high NAO index, cause deep convection and the production of homogenous mode waters of varying density classes (Brambilla and Talley, 2008a). Two main density classes of mode water meet at the Reykjanes Ridge. First, the isopycnals of the denser mode water (potential densities, σ_θ, around 27.55) have their winter surface outcrop in the southern Irminger Sea and Labrador Seas, and the characteristic of this water mass is therefore modified by air-sea interaction over these regions. This water type is hereafter termed Western Mode Water (WMW, Fig. 1). Second, the long-term trend of the lighter mode water ($\sim$27.45σ_θ, here termed Eastern Mode Water, EMW, Fig. 1) core properties is determined by the relative contribution of water from the subtropical gyre and the SPG, respectively (Hátún et al., 2005; Thierry et al., 2008) as well as by air-sea interactions along the eastern flank of the Reykjanes Ridge, and around the northern periphery of the Iceland Basin (Brambilla et al., 2008b; Thierry et al., 2008). The subarctic front marks the boundary between WMW and EMW in the Irminger Sea, and between EMW and more stratified waters in the central Iceland Basin - Labrador Sea Water (LSW) at depth and a lighter water type above (Fig. 1). The subpolar front determines the position of the Irminger Current and the main flow in the Iceland Basin. The transit time of WMW and the even denser LSW, from the Labrador Sea into and north through the Irminger Sea is about a year, which gives some prediction potential to this system (Deshayes et al., 2007; Sy et al., 1997; Yashayaev et al., 2007).

The convective western part of the SPG is a large nutrient reservoir and a center of abundance for *Calanus finmarchicus* (Heath et al., 2008) (Fig. 2). The mixing of WMW into the EMW, along the subarctic front in the northeastern Irminger Sea (Despres et al., 2011), will enrich the warmer and more saline EMW with nutrients and thus fuel primary production (Sanders et al., 2005). *C. finmarchicus* diapause at depth during winter, and high abundances are observed near the interface between EMW and the WMW/LSW the frontal zone of the NE Irminger Sea, and near the boundary between EMW and both LSW and the Iceland-Scotland Overflow Waters (ISOW) in the Iceland Basin (Gislason and Astthorsson, 2000; Heath et al., 2008). These animals start mating during their ascent toward the surface waters in March–April (Gislason et al., 2000). Eggs and larvae are produced in the surface layers and are an important food item for larger zooplankton (e.g. euphausiids, Silva et al., 2014) and fish larvae (e.g. cod and redfish larvae, Bainbridge and McKay, 1968).

On the shelf, *C. finmarchicus* provide likewise an efficient trophic pathway from primary producers to higher trophic levels (Gislason et al., 2000). The south Iceland shelf is devoid of *C. finmarchicus* during winter, and must therefore be repopulated during spring from the overwintering populations (Gislason and Astthorsson, 2000). The NW Iceland Basin has been suggested as the principal oceanic source, because the influx of oceanic water is likely to be most direct there (Valdimarsson and Malmberg, 1999), but advection of animals from the Irminger Sea is also possible (Gislason and Astthorsson, 2000).

The general biological production, ranging from *C. finmarchicus*, through euphausiids and fish is much higher in the NE Irminger Sea, compared to the NW Iceland Basin (Gudfinnsson et al., 2014). For example, the main redfish (*Sebastes mentella*) spawning grounds are closely aligned with the frontal zone along the western side of the Reykjanes Ridge (dark gray in Figs. 1 and 4) (Pedchenko, 2005) and hooded seals (*Cystophora cristata*), likely praying on

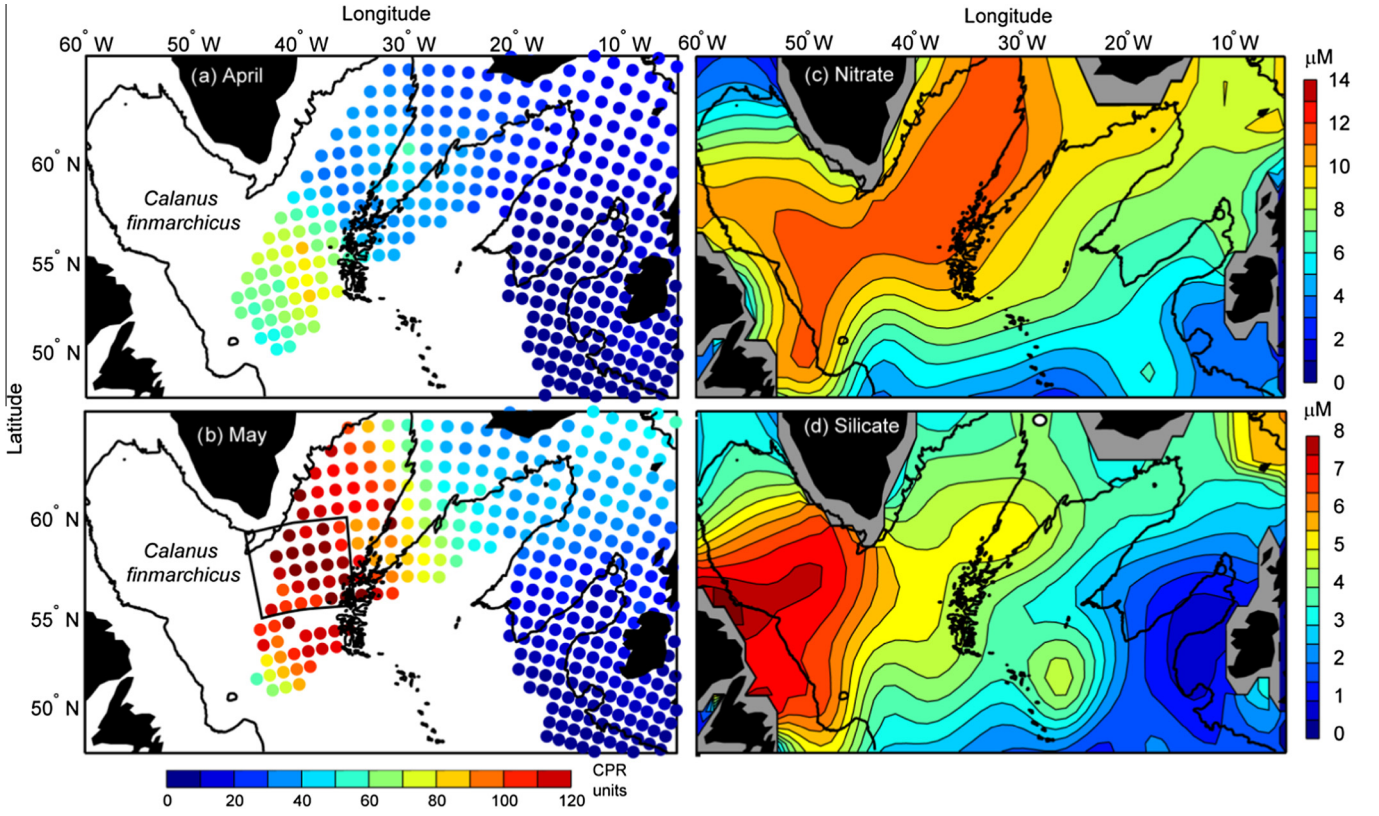

Fig. 2. The subpolar gyre – a source region. Average (1958–2005) near-surface *C. finmarchicus* (stages C5 and C6) abundance for (a) April and (b) May, observed by the Continuous Plankton Recorder (CPR) survey. Climatological nutrient distribution from the World Ocean Atlas (Garcia et al., 2010) at 50 m depth in June. (c) Nitrate and (d) silicate. The rectangle in (b) shows the region from where the individual CPR time series in Fig. 9 were selected. The 2000 m isobaths is shown for reference.

redfish (Folkow and Blix, 1999), also congregate here in spring (Folkow et al., 1996). Furthermore the densest concentrations of baleen fin whales (*Balaenoptera physalus*), feeding on euphausiids, are observed along the front around the northern tip of the SPG limb in the Irminger Sea (Víkingsson et al., 2009). The convective interior of the SPG limb in the Irminger Sea must be highly productive as well, since both redfish (Pedchenko, 2005) and the fin whales (Víkingsson et al., 2009) feed there during the summer, and the surface-feeding seabird black-legged kittiwake, (*Rissa tridactyla*) from populations as far away as the Barents Sea, congregate there during winter (Frederiksen et al., 2011).

Here, we suggest that an eastward 'spill-over' from the productive NE Irminger Sea might add to the biological production of the south Iceland shelf. Such a 'spill-over' would have to oppose the generally accepted mean westward flow over the northern Reykjanes Ridge (Valdimarsson and Malmberg, 1999). However, as shown by surface drifters, the ratio of Ekman to geostrophic flow velocity is particularly large over the Reykjanes Ridge (Flatau et al., 2003), and drifters flowing northward in the Irminger Current, along the western flank of the Reykjanes Ridge, can certainly end up on the eastern side of the ridge (Reverdin et al., 2003).

C. finmarchicus prey primarily on relatively large and fast-growing diatoms (Meyer-Harms et al., 1999; Nejstgaard et al., 1997). The silicate requiring diatoms lose their competitive advantage against smaller non-siliceous phytoplankton when silicate concentrations fall below 2 µM (Egge and Aksnes, 1992). The limiting silicate level occurs every year around May–June over the Reykjanes Ridge and are estimated to be a month or two later in the northern Irminger Sea (NIS hereafter) (Henson et al., 2006). Nutrient concentrations in the oceanic waters south of Iceland determine the nutrient content of Iceland shelf water, due to influxes onto the shelf (Stefánsson and Ólafsson, 1991). Shortly after the spring bloom, the strong primary production on the south Iceland shelf is, silicate limited (Stefánsson and Ólafsson, 1991). The severity of this silicate depletion should be expected to vary from year to year since the nutrient concentrations, in the oceanic waters off the shelf, are highly variable (Stefánsson and Ólafsson, 1991).

Large-scale changes in *C. finmarchicus* abundance in the north-eastern Atlantic have previously been linked to shifts in the major gyre circulations on decadal to multi-decadal time scales (Hátún et al., 2009a), and most recent studies on open-ocean climate and ecosystems focus on this long term, variability (Alheit et al., 2014; Nye et al., 2014), as well as the marked mid-1990s shift (Alheit et al., 2012; Hátún et al., 2009a,b). Sub-decadal variability, which in addition characterizes both physical and biological aspects of this system (Gaard et al., 2002; Larsen et al., 2012), has received less attention than the long-term variability. The gyre circulation, water mass composition and thus salinity variability is also characterized by marked 'dips', referred to as Great Salinity Anomalies (Belkin, 2004; Dickson et al., 1988). This sub-decadal variability is also evident in the biological productivity of the adjacent shelf ecosystems (Frederiksen et al., 2007; Gaard et al., 2002; Gislason et al., 2014).

Here, we focus on the marked sub-decadal variability in the NIS, Reykjanes Ridge and Iceland Basin region, and its potential oceanic impact on the south Iceland shelf ecosystem. The hypothesis to be tested is: *A north-eastward extended subpolar gyre improves the biological productivity southwest of Iceland – both oceanic and on the shelf.* The observational and model data used in our study are presented in Section 2. A generalized model and a suite of selected explanatory variables (*key metrics*) are presented in Section 3. In Section 4, these key metrics are investigated for their ability to explain the characteristic sub-decadal variability. The results are discussed in a larger context in Section 5 and brief conclusions are outlined in Section 6.

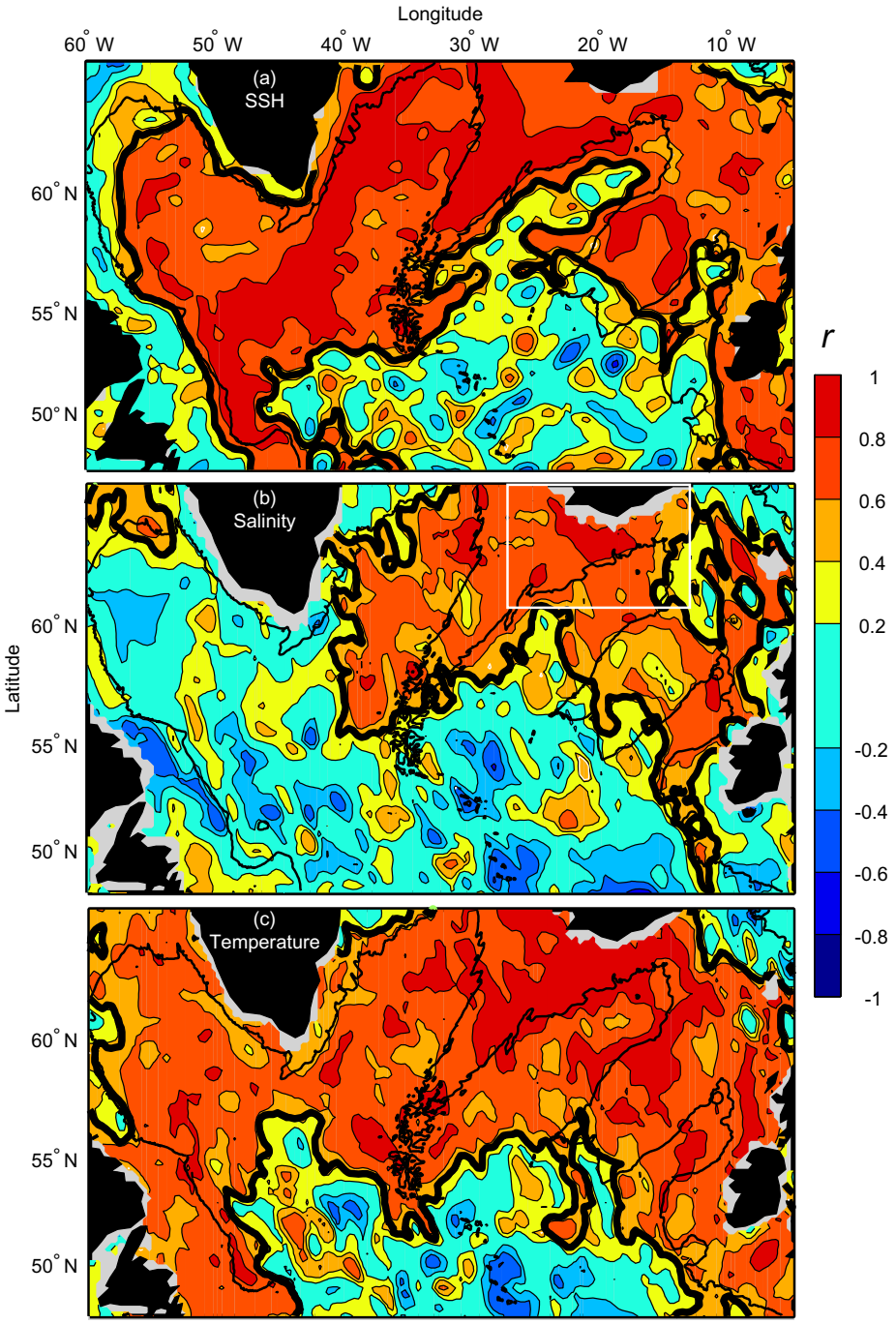

Fig. 3. Model validation. (a) Correlation coefficient (r) map between satellite altimetry, and the simulated sea surface height (SSH). Annual values during the period 1993–2012 are used. Panels (b) and (c), show correlation coefficients between observed (CliSAP) and simulated salinities and temperatures, respectively. Data are averaged over the upper 650 m of the water column, or, where it is shallower, down to the seafloor. Annual values during the period 1985–2005, are used. The periods are determined by data coverage. All datasets have been gridded onto the altimetry grid (Section 2.7) prior to the analysis. The thick black contour lines shows the 5% significance levels found by transforming the correlations to create a t-statistics having $N-2$ degrees of freedom, where N is the number of years. The white rectangle in (b) shows the region (60–65°N, 30–15°W) over which the salinity data were averaged in order to obtain the time series in Fig. 7b, and the 2000 m isobath is shown for reference.

2. Material and model validation

2.1. Satellite altimetry

Weekly averaged sea surface height (SSH) data were acquired from AVISO (http://www.aviso.oceanobs.com). The Mapped Sea Level Anomaly (MSLA) data combine altimeter data from TOPEX/Poseidon, Jason-1, EnviSat, and GeoSat which are mapped onto a 1/3° Mercator grid. For our analysis, the data have been averaged to annual fields.

2.2. The CliSAP hydrographic database

The observational data set from the CliSAP (Integrated Climate System Analysis and Prediction) data center (https://www.cen.uni-hamburg.de/facilities/data-center.html), used in this study, consists of about 800 000 hydrographic stations with water samples and/or CTD measurements from 1950 to 2006 in the region of 35°N to 70°N and 85°W to 10°E.

Data sources are WOD05 (World Ocean Database 2005, Boyer et al., 2006), HydroBase2 (Curry, 2002), ICES (International Council

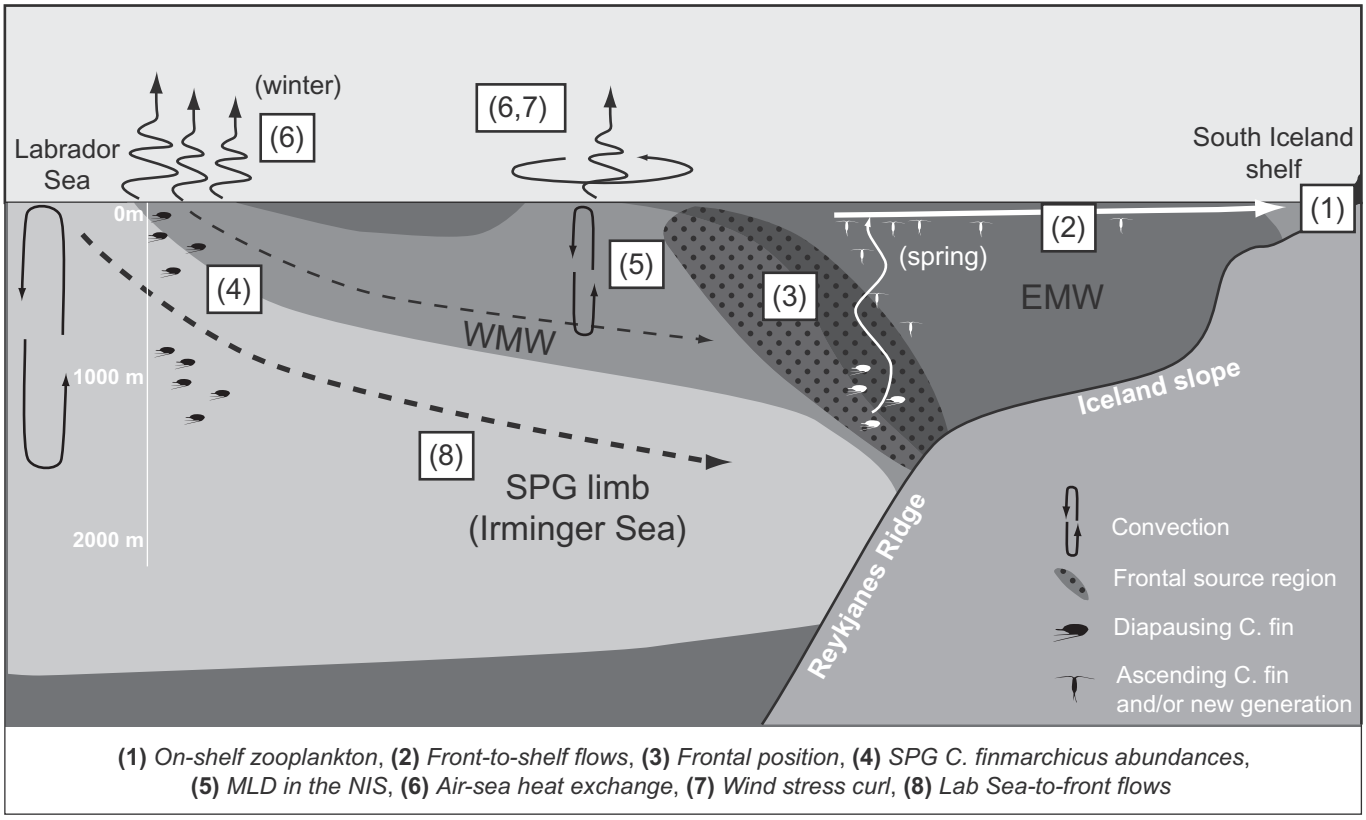

Fig. 4. A conceptual transect from the Labrador Sea and onto the south Iceland shelf. The numbers refer to the discussed metrics (see Table A1).

for the Exploration of the Sea), WOCE (World Ocean Circulation Experiment), CLIVAR (Climate Variability and Predictability Programme), and others. Additionally, about 30,000 float profiles from the Argo project (pilot program of the Global Ocean Observing System) between 1998 and 2006 were used. The temperature and salinity data were inspected for erroneous data, then selected at 82 pressure levels and averaged for each year in $1° \times 1°$ geographical boxes. Each box time series was then filtered with a 3-year running mean, yielding 55 3-year intervals between 1950 and 2006, which increases the spatial data density in each interval. This dataset has for example been used to investigate meridional shifts of the Gulf Stream/NAC system in the Newfoundland Basin (Muller et al., 2015; Nunez-Riboni et al., 2012).

2.3. Zooplankton data on the Iceland shelf

Zooplankton data were sampled during late May and early June 1971–2013 at five stations along a transect extending from the coast and beyond the shelf edge south of Iceland (Fig. 1). From 1970 to 1991, the samples were collected with a standard Hensen net (0.42 m^2 mouth area, 200 μm mesh size), whereas after that all the samples were collected using a WP2 net (0.25 m^2 mouth area, 200 μm mesh size). The nets were towed from 50 m to the surface with a speed of ~1 m s^{-1}. As the bottom depth at the shallowest station is only 46 m, the net could only be towed there from about 40 m. The volume of water filtered was measured with HydroBios flowmeters fitted in the mouth of the net. For the present analysis, we use data on zooplankton dry weight biomass standardized per m^3 averaged across all stations. Until 2001 the volume of zooplankton samples was measured at sea and the dry weight calculated using a conversion factor from Matthews and Heimdal (1980). From 2002 onwards the samples were deep frozen at sea and dried and weighed on shore (Postel et al., 2000). The copepod *C. finmarchicus* usually constitutes the dominant component of mesozooplankton biomass in the samples (Astthorsson and Gislason, 1995).

2.4. Oceanic zooplankton data from the CPR

Additional plankton data were obtained from the Continuous Plankton Recorder (CPR) survey (Batten et al., 2003). The survey is a monitoring programme that uses the CPR sampling device, towed at ~10 m depth behind ships of opportunity on standard routes. The CPR data provide a good representation of the uppermost 20 m of the water column, and thus of the epipelagic zone. As the CPR samples are highly heterogeneous in space and time, spatial interpolation using the inverse squared distance method (Lam, 1983) was applied to obtain gridded datasets for further analysis. Only data for the adult *C. finmarchicus* copepodite stages C5 and C6 were used in this study. Annual averages were calculated for each grid point by first interpolating missing months linearly, and then averaging the months March–October; outside this period the species has low abundances. Years with more than two missing months were omitted and grid points with more than 20 missing years were disregarded. Other ways of calculating annual averages were also tried (no temporal interpolation, anomalies from the mean seasonal cycle), and the resulting time series showed similar periods of high and low abundance.

2.5. Atmospheric reanalysis

Ocean–atmosphere heat and momentum fluxes from the National Center for Environmental Prediction/National Center for Atmospheric Research (NCEP/NCAR) reanalysis project (Kalnay et al., 1996) were used to investigate the atmospheric impact on the observed zooplankton variability and the simulated mixed

layer depths. Averages over the late winter months, January–March, were used in the analyses.

2.6. The Max Planck Institute Ocean Model (MPI-OM)

The ocean-sea ice model used in this study is the Max Planck Institute for Meteorology ocean general circulation model MPI-OM (Jungclaus et al., 2013; Marsland et al., 2003). MPI-OM is a free-surface primitive equation model formulated on orthogonal curvilinear coordinates and includes a Hibler-type dynamic-thermodynamic sea-ice model. Stand-alone MPI-OM simulations forced with atmospheric reanalysis fields have been used to assess and study decadal-scale variability in the subpolar North Atlantic (Muller et al., 2015; Nunez-Riboni et al., 2012). The grid-configuration applied in the present study features a nominal resolution of 1.5°, with the northern grid pole located over Greenland (to avoid grid singularities in the computational ocean domain). The convergence of the mesh-size toward the poles translates into a grid spacing of 15–50 km in the area of interest (subpolar Atlantic). Vertically, 40 irregularly spaced z-levels are used with the first 20 levels covering the upper 700 m of the water column.

The MPI-OM simulation (Matei et al., 2012a,b) used in the present study is forced with daily surface fluxes of heat, freshwater and momentum obtained from the NCEP/NCAR reanalysis (Kalnay et al., 1996). The heat flux was not taken directly from the reanalysis fields, but rather computed interactively using bulk formulas as described in Marsland et al. (2003). The model sea surface salinity is relaxed toward the Levitus climatology (Levitus, 1998) with an e-folding time of 30 days to correct for unbalanced globally integrated surface freshwater flux. The MPI-OM is initialized with annual-mean temperature and salinity from the Levitus climatology (Levitus, 1998) and mean velocities at rest and integrated for 10 consecutive cycles, each covering the period 1948–2007. The first six cycles are considered as a spin-up period and cycle number seven is analyzed. For more details about the MPI-OM simulation, the reader is referred to Matei et al. (2012b).

2.7. Model validation

2.7.1. Sea surface height validation

Satellite altimetry is a well suited dataset against which to validate the large scale dynamics of the model. SSH integrates the density of the whole water column (Siegismund et al., 2007), and the gradient of the SSH field reflects the surface currents (Hátún and McClimans, 2003). We have correlated annual averages of the observed and simulated SSH for the period 1993–2012. The resulting correlation map shows close co-variability in the Labrador and Irminger Seas, Reykjanes Ridge as well as for the region southwest of the Faroe Islands (Fig. 3a, reddish colors, $r > 0.6$). The lower correlations in the south-eastern subpolar region are due to strong eddy activity there associated with the NAC (Heywood et al., 1994), which the non-eddy-resolving model configuration used here cannot capture. In addition, the NAC system generally appears too far south and too zonal in this model system, a common systematic bias of non-eddy-resolving ocean models. Away from continental slopes, the simulated SSH is closely correlated ($r > 0.95$) with the steric height, calculated using the simulated temperatures and salinities over the upper 2000 m (not shown), which is in agreement with observations (Siegismund et al., 2007). The spatial correlation map between the simulated steric height and the altimetry is therefore almost identical to Fig. 3a.

This indicates (*i*) that the simulations realistically represent the hydrography in the region of interest during the altimetry period (1993–2012) and (*ii*) that the altimetry data over open-ocean regions, also used to calculate the gyre index (Häkkinen and Rhines, 2004), can be used as a 'buoyancy meter'.

2.7.2. Hydrography validation

It is not trivial to make a true large-scale validation of hydrography, since the subpolar region has been sparsely sampled, especially during the pre-Argo era (before 1998, www.argo.net). We have correlated mean upper-ocean (0–650 m) temperature and salinity from the CliSAP hydrographic dataset with the corresponding simulated quantities for the period 1985–2005. This limited time-period is chosen because of the sparse data coverage prior to 1985. The resulting correlation maps of salinity and temperature show that the model simulation provides a reasonable representation of the observed hydrography within the Irminger Sea, the Reykjanes Ridge and the NW Iceland Basin region (Fig. 3b and c). Areas showing weak correspondence between simulated and observed salinity fields reflect not only model deficiency, but possibly also data limitation, especially over the very sparsely sampled Labrador Sea region. The negative correlations in the southern part of our domain might be related to the unrealistic position of the NAC in the model simulation. In summary, the model performs satisfactorily within the focus region of this study, southwest of Iceland.

2.7.3. Mixed layer depth

The mixed layer depth (MLD) is likely a key oceanic quantity, impacting the production and life cycle of zooplankton (Backhaus et al., 2003), as discussed below (Section 4.3). The simulated MLD cannot be spatio-temporally validated against observations, since measured data do not exist at the temporal and spatial scales considered here.

3. Working hypothesis and approach

Our hypothesis, presented in Section 1, is tested using a selection of key metrics, which reflect the potential impact of a variable subpolar gyre on salient physical and zooplankton parameters southwest of Iceland. These key metrics are emphasized in italic font below, and the numbers refer to the summary given in Table A1 and the illustration in Fig. 4.

The *On-shelf zooplankton* (metric 1, Fig. 9) is mainly reflecting the dryweight of *C. finmarchicus* (Section 2.3) on the south Iceland shelf (Fig. 1). This is expected to depend on the oceanic zooplankton concentration as well as on the distance and the transports from the shifting frontal source in the Reykjanes Ridge region to the shelf, determined by the *Front-to-shelf flows* (metric 2, Section 4.1) and the *Frontal position* (metric 3, Section 4.2). The surface layer abundance of *C. finmarchicus* during the ascent and reproductive phase in March–May is likely regulated by convective activity. Near-surface data from the CPR survey is used as the *SPG C. finmarchicus abundance* (metric 4, Section 4.3). The convective activity, here proxied by the *MLD in the NIS* (metric 5, Section 4.3), will depend on local *air-sea heat exchanges* (metric 6) and the action of regional *wind stress curl* (metric 7) in the same winter (Section 4.4). Strong *air-sea heat exchange* in the Labrador-south Irminger Seas induces deep convection and production of unstable (weakly stratified) WMW, which will precondition the NIS after about a year, due to horizontal advection – hereafter termed *Lab Sea-to-front flows* (metric 8, Section 4.5). A northward influx of overwintering animals from near the center of abundance in the western SPG, transported in the *Lab Sea-to-front flows* may be an important source.

Similar processes might also regulate the amount of nutrients advected from the SPG onto the shelf, which will have a bottom-up impact on the summer primary production of, both oceanic and on-shelf waters.

The actual cross-shelf influx of zooplankton is given as a multiplication of the cross-shelf exchanges of waters (Q) and the

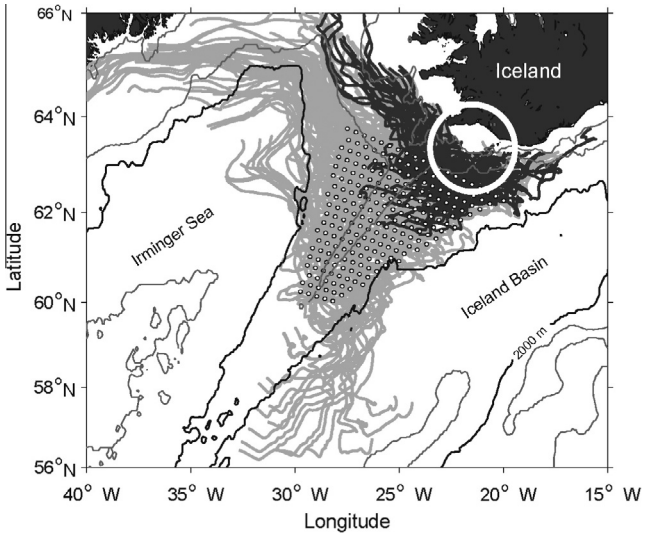

Fig. 5. The *Front-to-shelf flows* (metric 2, Fig. 4, Table A1). Flow trajectories for particles seeded at 6 m depths within a triangle covering the northern part of the Reykjanes Ridge (white dots, every other seeding point shown) illustrated for a year with average flows toward the shelf (2002). The gray-shading shows all trajectories and black threads shows those that pass through the target region, which is illustrated with the white circle. The 200 m, 500 m, 2000 m (thick black line) and 3000 m isobaths are shown for reference.

off-shelf concentration of zooplankton (C). We limit our scope to demonstrate covariability between the *On-shelf zooplankton* and C. Proper analysis of Q would require very high-resolution models and/or observations, which is beyond the scope of the present work.

4. Results

4.1. Front-to-shelf flows

The strongest increase in the near-surface abundances of *C. finmarchicus* are typically observed during April (Fig. 2a and b). To examine possible transports of copepods from the overwintering regions toward the slope, 'particles' were seeded into the simulated flow field. This was done once a week during April, every year (1970–2010) at six meters depth, in a region east and west from the summit of the Reykjanes Ridge, shallower than 2000 m (Appendix A.1 and Fig. 5). This experiment shows that although most of the particles flow northwest, as expected from the generally accepted flow pattern (Valdimarsson and Malmberg, 1999), there is an important northeastward near-surface flow toward the south Iceland shelf as well (Fig. 5). The origin of the particles which reach the target region (white circle in Fig. 5) before mid-June is shown in Fig. A.1a, as the percentage of all particles seeded in April for all years. A large fraction of the near-surface water over the northern Reykjanes Ridge can flow eastwards along the Selvogsgrunn slope before late May-early June, when the on-shelf zooplankton observations are made. The numbers of seeded particles, which reach the near-shelf target region (Fig. 5) before mid-June each year, varied from the than 10% to more than 40% (Fig. A.1b). Thus we conclude that variable Front-to-shelf flows may contribute to the variability of the on-shelf zooplankton biomass.

4.2. The position of the sub-arctic front

In addition to the flows, the distance from the source region to shelf might also vary. Due to the overwintering *C. finmarchicus* in Atlantic water, or aligned with the transition zone between EMW and LSW (Gislason and Astthorsson, 2000; Heath et al., 2000), the *Frontal position* (metric 3, Fig. 4, Table A1) is expected to reflect shifts in the distribution of zooplankton along both sides of the Reykjanes Ridge.

SSH variability is largely determined by the average density of the entire water column (Section 2.7.1), and frontal shift and the large density contrast between different classes of mode waters induces particularly large SSH variability in the frontal zone (Richter et al., 2012). The Empirical Orthogonal Function (EOF) analysis of the simulated SSH field (Miami Isopycnal Coordinate Ocean Model, MICOM, Bleck et al., 1992; Sandø and Furevik, 2008) over the North Atlantic, previously used to calculate the so-called gyre index (Hátún et al., 2005, Fig. 6), reflects such mode water variability. The first EOF mode is associated with the highly variable mode water volume in the Reykjanes Ridge region, and thus the position of the boundaries between EMW, WMW and LSW, (whitish colors in Fig. 6a). The temporal variability of this pattern is represented by the gyre index (Fig. 6c, full), where high values (as plotted) are associated with the dominance of denser water types - a spatially large SPG. A similar EOF analysis has been applied to the SSH field derived from the MPI-OM experiment. The MPI-OM-derived gyre index is closely correlated with both the MICOM-derived ($r = 0.70$, $P < 10^{-7}$) and the altimetry-derived ($r = 0.89$, $P < 10^{-7}$) gyre index (Fig. 6c). The associated spatial pattern (Fig. 6b) is comparable to the previous MICOM (cf. Fig. 6a and b) and altimetry analyses (Häkkinen and Rhines, 2004). This result shows that (*i*) there is consistency between both model systems and (*ii*) the simulated variability is realistic.

The MICOM-derived gyre index has previously been compared to the observed temperature and salinity at a standard station in the NIS, showing clear sub-decadal variability masked by more conspicuous long-term variability - salinity drops occur during the years when the SPG expands northeastwards (Hátún et al., 2005). The observed (upper 200 m, CliSAP) salinity from the broader NE Irminger Sea-northern Reykjanes Ridge-NW Iceland Basin region (box in Fig. 3b) likewise shows marked reductions during the periods when the subpolar gyre is strong (Fig. 7b, $r = 0.63$, $P < 10^{-5}$).

To further illustrate how the gyre index is associated with zonal shifts of the main subarctic front in the NIS, annual averaged observed salinity (CliSAP) at 100 m depths along a section crossing the Irminger Sea at 60.5°N (Fig. 6a), is plotted as a Hovmöller (longitude-year) diagram (Fig. 7a). The marked east-west fluctuations of the isohalines are closely correlated with the MPI-OM-derived gyre index ($r > 0.74$, $P < 10^{-7}$, lag = 6–8 months, when using the 35.0 isohaline).

Based on the association between the gyre index and shifts of the subarctic front, we here use the high-pass filtered gyre index, calculated from the MPI-OM simulation, as our *Frontal position* metric (Table A1). The *Frontal position* is highly correlated with the *On-shelf zooplankton* (1) record (Fig. 6d and Table 1). Years when the front in the NIS shifted toward the east (low salinities along the 60.5°N section) generally coincide with increased zooplankton abundances on the south Iceland shelf (Fig. 7a). The zooplankton peak around 1990 is an exception to this pattern. The *Frontal position* is therefore a plausible link to the *On-shelf zooplankton* abundance.

4.3. Mixed layer depth and C. finmarchicus abundances

As the gyre index reflects shifts of the main water mass boundaries, and thus the volumes of WMW and EMW, respectively (Thierry et al., 2008), the shorter term variability identifiable in the gyre index is likely associated with convective activity and the MLD (Brambilla et al., 2008b). Strong convection may be

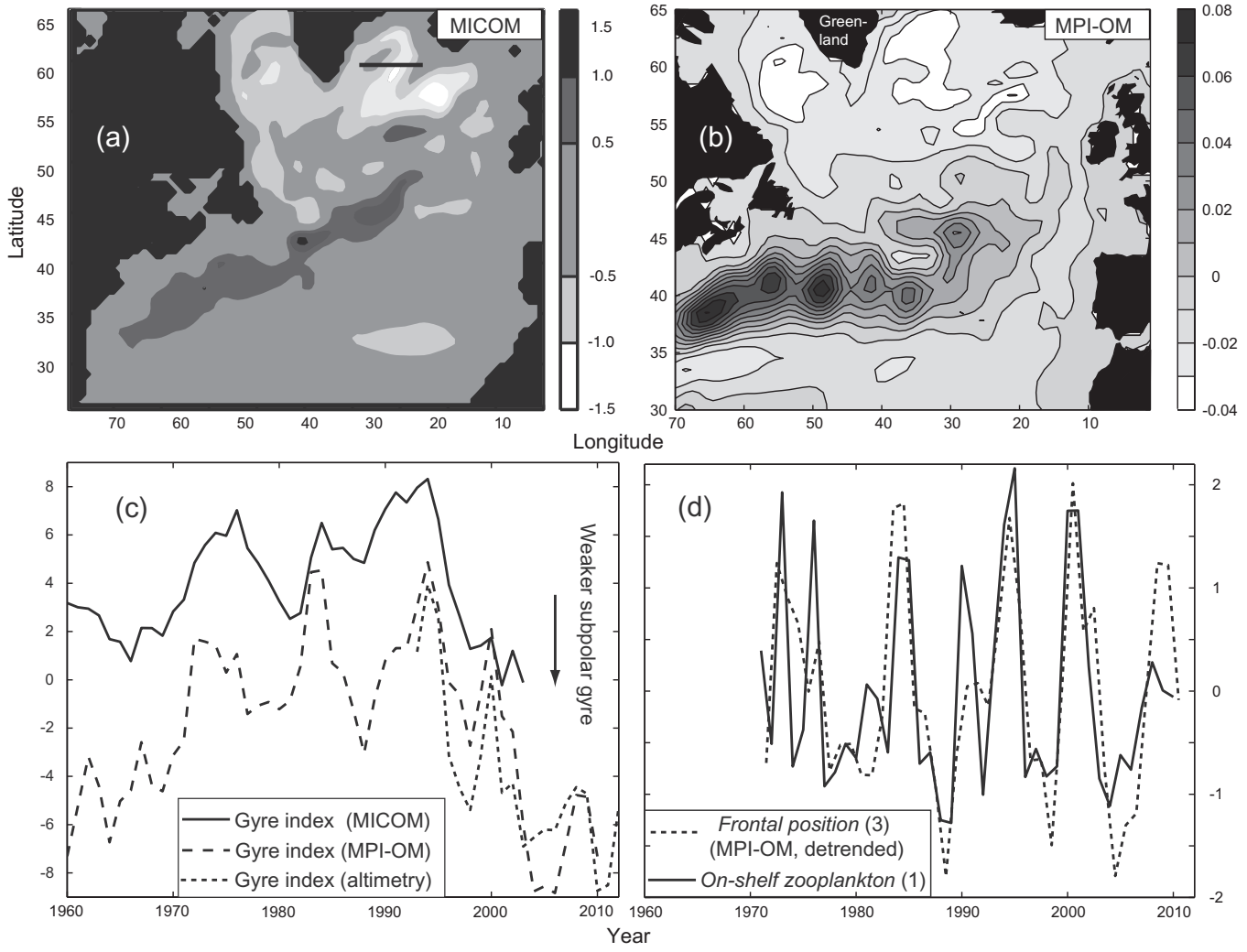

Fig. 6. Large-scale perspective. Spatial patterns from EOF analyses of simulated sea surface heights obtained from (a) a previous analysis of MICOM (see text) and (b), the presently employed MPI-OM run. (c) An altimeter-based gyre index (dotted, Larsen et al., 2012), and the gyre indices obtained from MICOM (full, Hátún et al., 2005) and MPI-OM (dashed), respectively (not to scale). (d) The *Frontal position* (dotted) and the *On-shelf zooplankton* (metric 1, full line, not to scale). The *Frontal position* (metric 3, Fig. 4, Table A1) is the high-pass filtered MPI-OM based gyre index. The east–west line in (a) shows the section from where the observed salinities in Fig. 7a were selected.

beneficial for the oceanic zooplankton community in several ways (Backhaus et al., 2003) (see Section 5), thus a possible link to convection is investigated using winter MLD as a proxy.

The *On-shelf zooplankton* (1) is highly correlated with the MLD on the northeastern flank of the Reykjanes Ridge, throughout the Irminger Sea and into the Labrador Sea, as well as the water south of the Iceland-Faroe Ridge. This is demonstrated by correlating the zooplankton record against the simulated March MLD at each MPI-OM grid point (Fig. 8). The correlations are particularly high and spatially homogeneous in the Irminger Sea, likely caused by the broad surface outcrop of the WMW during winter. Because MLD variability in the Irminger Sea is stronger than in the Iceland Basin, and since the model performance is generally good in the Irminger Sea (Fig. 3), a *MLD in the NIS* metric (Table A1) is constructed by averaging the simulated March MLD values over a box in the NIS (Fig. 8).

March values are used, since the deepest mixing most often occurs during this month caused by the integrated effect of the winter air-sea forcing. The *MLD in the NIS* is correlated with the gyre index ($r = 0.76$, $P < 10^{-9}$), but emphasized more the inter-annual variability.

Likewise, time series of annually averaged *C. finmarchicus* for a region in the convective southern Irminger Sea show mostly inter-annual variability (Fig. 9), and less long-term changes compared to the previously reported *C. finmarchicus* variability farther east (Hátún et al., 2009a). The *SPG C. finmarchicus abundance* (metric 4) is calculated as an average of the CPR time series within the rectangle in the south Irminger Sea, shown in Fig. 2b. This metric is significantly correlated to the *MLD in the NIS* (Fig. 9) ($r > 0.76$, $P < 10^{-9}$, lag = 4–7 months, see Appendix A.2), indicating that deep convection during winter does lead to high zooplankton abundance in the following production season. The shelf zooplankton community has to be repopulated from the oceanic *C. finmarchicus* stock every spring (Gislason and Astthorsson, 2000), and the *On-shelf zooplankton* is also tightly correlated with the SPG *C. finmarchicus* abundance (Table 1, Fig. 9). All peaks in oceanic *Calanus* measured by the CPR, occurring during the years 1973, 1976, 1984–1985, 1991, 1993–95 and 2000–2001, had their counterpart in the shelf concentrations derived from Henson net/WP2 net sampling.

4.4. Atmospheric forcing

The marine climate south of Iceland is, in addition to local atmospheric forcing, also influenced by remote air-sea interactions, advected to the region via the WMW and the EMW.

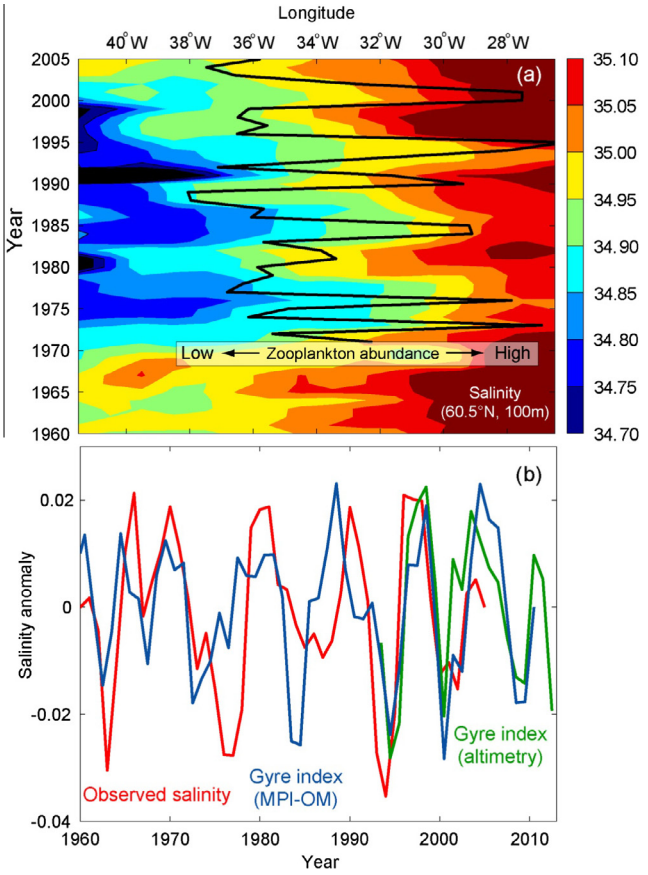

Fig. 7. Observed sub-decadal salinity variability south of Iceland. (a) A Hovmöller diagram of the observed salinity at 100-m depths, along a section across the Irminger Sea and Reykjanes Ridge at 60.5°N (Fig. 6a) and the *On-shelf zooplankton* record (black, not to scale). (b) The annual averaged observed upper layer (0–200 m) salinity over the rectangle shown in Fig. 3b (red, extracted from the CliSAP hydrographic database) and the inverted gyre indices based on the MPI-OM simulations (blue), and satellite altimetry (Larsen et al., 2012), respectively. A high-pass filter with a 6-year cut-off has been applied to all series, in order to emphasize on the shorter-term variability.

The winter MLD appears to be a source of the characteristic high-low variability (Fig. 9), which is particularly identifiable in the Labrador-Irminger Seas (Fig. 8). The most direct physical drivers of mode water production are *Air-sea heat exchange* (6) and *Wind stress curl* (7) (Table A1, Fig. 4), both hidden in the widely used NAO index. To investigate the relative importance of these atmospheric drivers, the *MLD in the NIS* (5) has been correlated against *air-sea heat exchange* and *wind stress curl*, obtained from the NCEP/NCAR reanalysis fields, averaged over the late winter months (Jan–March) (Fig. 10). Regarding air-sea heat exchange, high correlations are found on the Reykjanes Ridge (Fig. 10a), but the correlation maximum appears in the Labrador Sea, around the southern tip of Greenland (Cape Farewell) and into the Irminger Sea ($r = 0.72$, $P < 10^{-10}$, when considering the region, 58–60°N, 47–43°W). This reflects the importance of direct atmospheric forcing, but also points to the importance of air-sea interactions upstream, which subsequently could impact the NIS through the *Lab Sea-to-front flows* (8) described below.

The *MLD in the NIS* is also correlated to the *Wind stress curl* around south Greenland, although weaker than the heat losses (Fig. 10b). The process is likely a spin-up of the so-called Irminger Gyre, through Ekman pumping (Deshayes et al., 2007). This lifts the isopycnals in the Irminger Sea toward the surface, destabilizes the water column and makes it more susceptible to deep convection (Pickart et al., 2003). This wind-induced tightening of the isopycnals might also influence the *Frontal position*, and the *Front-to-shelf flows*. The negative correlations west of the British Isles are associated with the marked meridional excursion of the zero wind stress curl there (Marshall et al., 2001), and is not directly related to the discussed processes in the Irminger Sea.

Although clear linkages between the *On-shelf zooplankton* (1) variability and important metrics in the open-ocean are demonstrated, one could still argue that there could be a common large-scale atmospheric driver which impacts the shelf waters and the open-ocean similarly, but independently. The correlations between the *On-shelf zooplankton* record and the *air-sea heat exchanges* are, however, only marginally significant for a region immediately southwest of Iceland (62–64°N, 26–20°W) and no link is found to local *wind stress (curls)* (Table 1), which underscores that zooplankton variability on the shelf is not primarily driven by local atmospheric forcing. In addition, the correlation between the summer sampled *on-shelf zooplankton* and the winter NAO index is both weak, and zooplankton peaks occur either during the same summer and/or the subsequent summer (a lag of 7–9 months on average, Table 1, Appendix A.1). This time-lag points to the importance of advective processes and preconditioning, since the thermal inertia and 'memory' on a shallow shelf must be short.

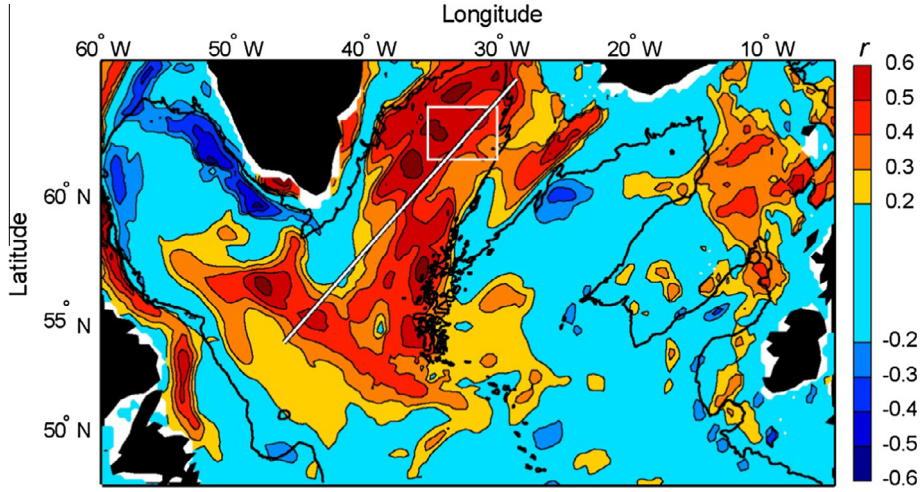

Fig. 8. Correlation coefficients (r) between the *on-shelf zooplankton* (black line in Figs. 6d and 7a), and the simulated March mixed layer depths (MLDs) at each model grid-point. The white rectangle refers to the box, over which the simulated MLD times series (Fig. 9) was averaged, and the white slanted line shows the section from where the simulated densities in Fig. 11 were extracted.

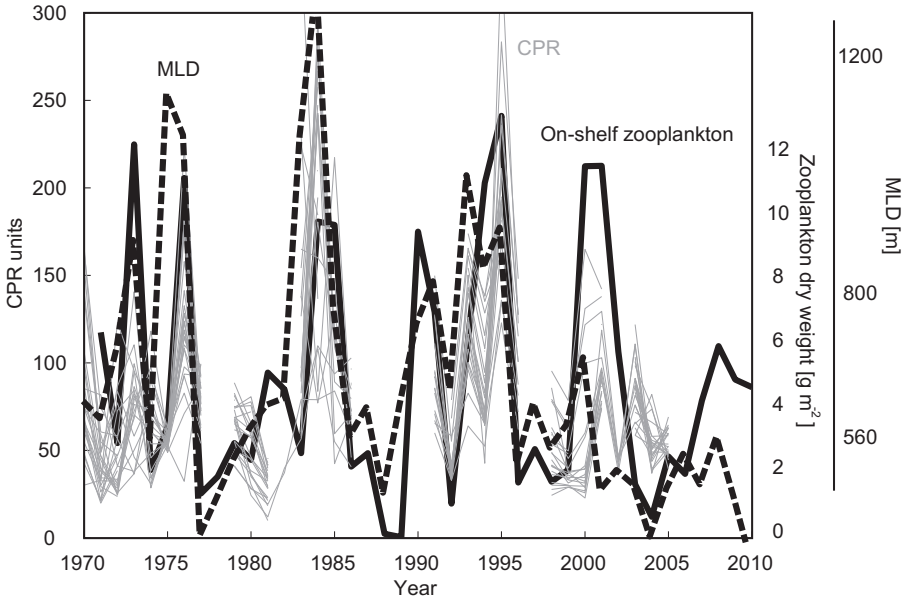

Fig. 9. *SPG C. finmarchicus abundances* (metric 4, thin gray lines, left axis) and the *MLD in the NIS* (metric 5, dashed line), and the *On-shelf zooplankton* (full line). Individual Continuous Plankton Recorder (CPR) time series of annually averaged *C. finmarchicus* within the polygon in the southern Irminger Sea (Fig. 2b) are shown. Gaps in the CPR data are due to periods when the survey was not operational.

Table 1
Lagged correlations (see Appendix A.1) between the *On-shelf zooplankton* metric (1), and the NAO and the other metrics (Table A1).

	Metric Statistics	NAO	*MLD in the NIS* (5)	*Air-sea heat exchange* (6)	*Wind stress curl* (7)	*SPG C. finmarchicus* (4)	Frontal position (3)
Original	*r*>	0.46	0.62	0.37	NS	0.56	0.80
	P<	0.02	0.00005	0.02	–	0.0004	2e−9
	Lag (months)	7–9	3–8	5–7	–	0	5–7
High-passed	*r*>	0.47	0.67	0.38	NS	0.58	n/a
	P<	0.002	3e−6	0.02	–	0.0003	n/a
	Lag (months)	7–9	4–6	5–7	–	0	n/a

NS: Not Significant.

4.5. From the Labrador Sea to the northern Irminger Sea

The remote action of convection in the Labrador-south Irminger Seas and *Lab Sea-to-front flows* (8) (Table A1) is expected to influence the *MLD in the NIS* (5) through its preconditioning effect, with an advective time-lag on the order of a year (Bersch et al., 2007; Yashayaev et al., 2007). Since these advective processes, and the time-lags induced, provide a potential for prediction of biologically productive years along the Reykjanes Ridge and on the south Iceland shelf, we have investigated them in more detail.

4.5.1. Density anomalies

First we illustrate the simulated density anomalies related to the formation and spreading of WMW and its linkage to the *MLD in the NIS* for the simulated period 1948–2010. Strong density anomalies are associated with deep convection in the Labrador-South Irminger Seas (at about 54°N in Fig. 11). The concurrence of these anomalies at the exit of the Labrador Sea and in the NIS is illustrated by the Hovmöller (latitude-time) diagram (Fig. 11) of the simulated annually averaged potential density (σ_θ) for the depth range of 220–420 m, along the section shown in Fig. 8. Monthly data reveal that these density anomalies are in fact advected north (not shown). There is a close correspondence between the presented MLD time series (Fig. 9) and the upper-ocean density in the NIS (61–63°N) (Fig. 11). The same general pattern, although more smoothed, is also seen when the deeper LSW layers are included (not shown). The detailed structure of the MLD time series, like e.g. the dual peak during the mid-1970s, is however not seen in the Labrador Sea, and must therefore be shaped by local air-sea interaction in the north. Periods with generally increased simulated MLDs in the subpolar region (Fig. 11) coincide with periods of increased convection observed in the Labrador Sea, both in the central part of the basin and just southwest of Greenland (near Cape Farewell) (Deshayes et al., 2007 and references therein). The advection of weakly stratified WMW preconditions the NIS, rendering the water column more susceptible for convection.

4.5.2. Lab Sea-to-front flows

The Lab Sea-to-front flows are further investigated by performing particle tracking experiments using the simulated flow fields. The potential preconditioning effect of WMW on the convective activity in the NIS is studied by seeding 1066 particles (tracers) at 420 m depths within a box in the southern Irminger Sea every 1st of March, 1970–2010 (Fig. 12a, Appendix A.2).

The results clearly illustrate the presence of a strong northeastward flow of WMW from the seeding region toward the NIS (Fig. 12a). The distribution of travel times taken by the particles to reach the NIS has two peaks, one at about a year, in agreement with observational studies (Bersch et al., 2007; Yashayaev et al., 2007) and another lower and broader peak at 24–28 months (Fig. 12b). A time series of the influx of WMW to the target region

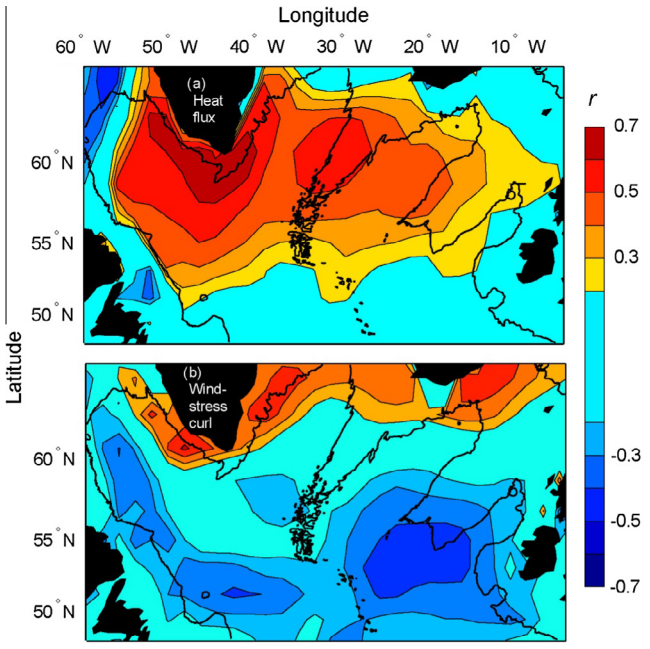

Fig. 10. Atmospheric forcing. Correlation coefficients (r) between the *MLD in the NIS* (metric 5, red line in Fig. 9) and (a) the *Air-sea heat exchange* (metric 6) and (b) *Wind stress curl* (metric 7), respectively – both fields averaged of the late winter months January to March. Positive correlation coefficients mean that increased MLD is associated with increased heat loss from the ocean, and cyclonic wind stress curl forcing. The 2000 m isobath is shown for reference.

(circle in Fig. 12a) is estimated by including all particles that reach the destination within the first 21 months (first main peak, black bars in Fig. 12b). Thus, we acknowledge that the preconditioning effect of a strong winter might last beyond the subsequent winter, while assuming that the broader 24–28 months peak will contribute less to the preconditioning. These *Lab Sea-to-front flows* vary considerably between years. In some years almost no particles seeded in the south reach the NIS, while nearly every second particle completes this journey in other years (e.g. 1993–1994) (Fig. 12c, gray bars).

There also appears to be increased *SPG C. finmarchicus abundances* during years when *Lab Sea-to-front flows* are enhanced (Fig. 12c), but this association is statistically weak ($r > 0.30$, $P < 0.08$, lag = 12–14 months).

Our results indicate that, in addition to the regional oceanography south of Iceland, *the Lab Sea-to-front flows* (8) might also impact the zooplankton dynamics in the NIS, primarily through its preconditioning effect on the MLD, and likely advection of nutrients as well, and potentially by transporting C. *finmarchicus* from the reservoir in the western SPG (Fig. 2).

5. Discussion

Calanus finmarchicus, which dominates the zooplankton biomass on the south Iceland shelf (Astthorsson et al., 1983; Gislason et al., 2009), is a key linkage to higher trophic levels in this ecosystem. No link has previously been identified between the characteristic 'high-or-low' on-shelf *C. finmarchicus* variability and neither local environmental parameters nor large-scale atmospheric forcing (NAO) (Gislason et al., 2014), while coastal zooplankton species are influenced by salinity and used nitrate, due to river efflux (Gislason et al., 2009). We also found no link to local *air-sea heat exchanges* (6) or *wind stress curl* (7), in our analyses of potential local forcing. It has been suggested, that variable influx of *C. finmarchicus* from core gyre regions to adjacent shelves regions around the subpolar Atlantic might regulate the on-shelf biomass of this species (Gislason and Astthorsson, 2000; Harms et al., 2000; Sundby, 2000). To investigate this suggestion, our study has provided support for our hypothesis that a northeastward

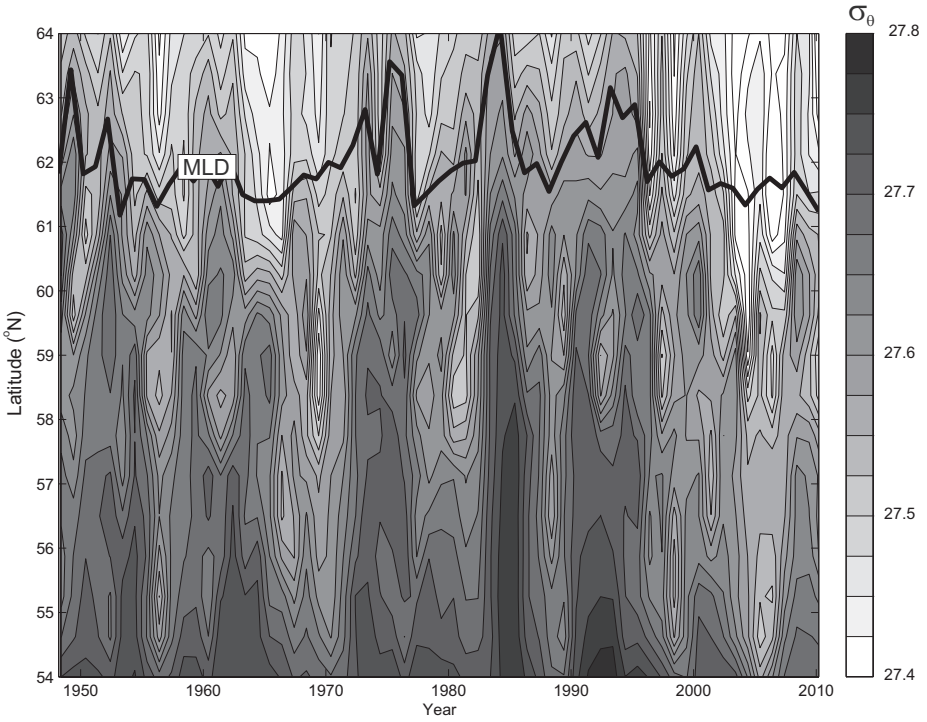

Fig. 11. Upper-layer density and MLD. Hovmöller (latitude-year) diagram of simulated annual potential density anomaly (σ_θ) within the 220–420 m depth range and along the section shown in Fig. 8. The *MLD in the NIS* is overlaid for comparison (thick line).

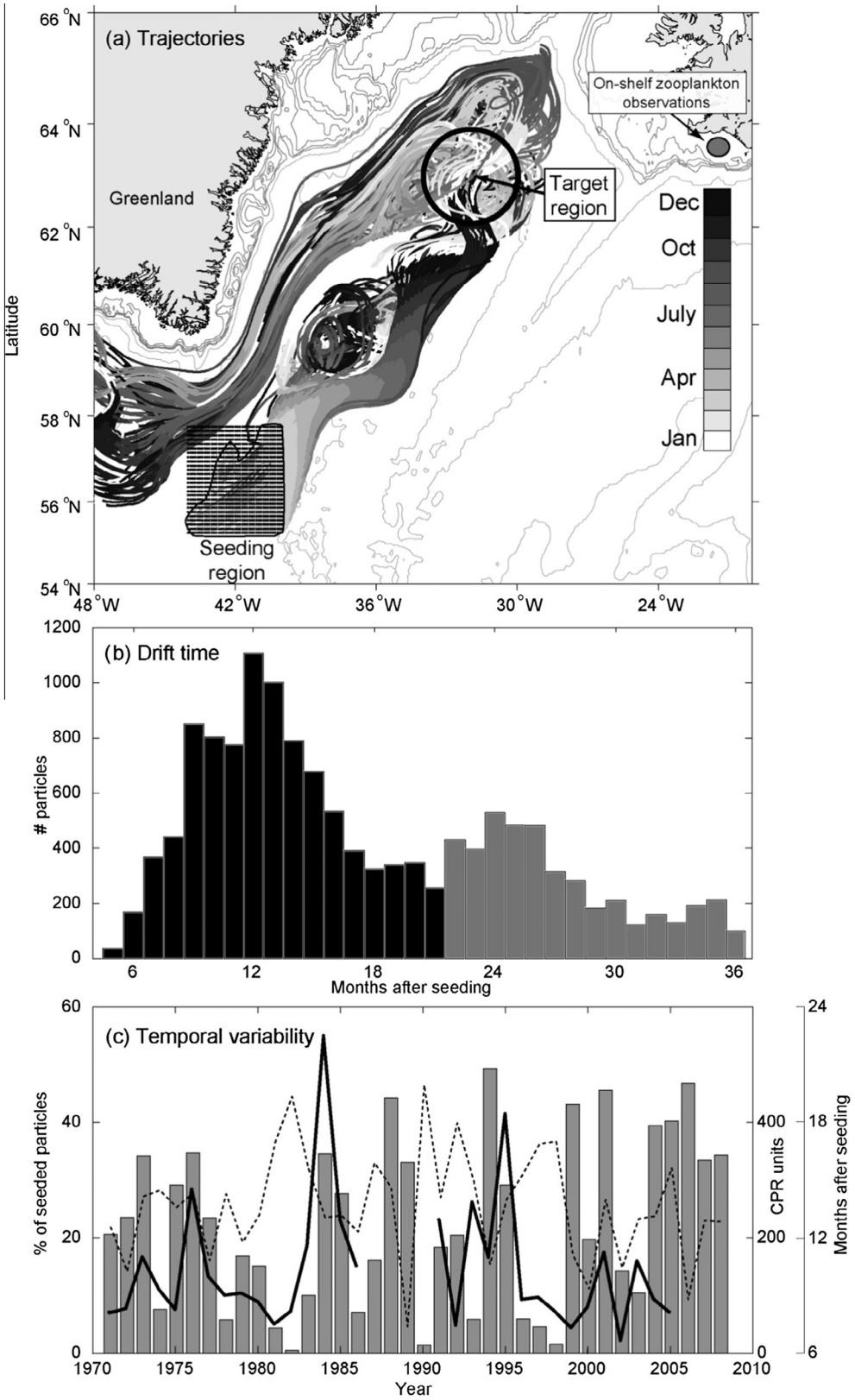

Fig. 12. The *Lab Sea-to-front flows* (metric 8, Table A1). (a) Flow trajectories for particles seeded at 420 m depths in the southern Irminger Sea during the first 21 months of drift, illustrated for a period with average flows (1975–76). The gray-shading refers to the months. The seeding region is shown with the black dots, and the target region is illustrated with the circle. Only particles that passed through the target region are shown. (b) Distribution of arrival times at the target region in the NIS – number of particle summed over the period 1970–2005. The number of particles seeded each year were 1066 (Table A2). (c) Temporal variability of the horizontal advection. The bars show the percentage of particles seeded, that reached the target region within the selected time-frame of 21 months - black bars in (b). The average drift time for each year, and the *SPG C. finmarchicus abundance* (average over the thin blue CPR series in Fig. 9) are shown with red and black lines, respectively.

extended SPG increases the zooplankton concentrations southwest of Iceland, both in the open ocean and on the shelf.

The close relationship between the *On-shelf zooplankton* and both the model-based *Frontal index* (Fig. 6d) and the observed position of the subarctic front (Fig. 7a), clearly shows that the production of *C. finmarchicus* southwest of Iceland depends on changes in the main mode waters. Large volumes of subarctic water masses and a northward shifted subarctic front (large SPG), results in a high biomass of *C. finmarchicus*.

Open-ocean marine climate in the subpolar Atlantic is, however, dominated by decadal to multi-decadal variability (Fig. 6c), which is not evident in the *On-shelf zooplankton*. In order to disentangle the importance of processes acting at multi-decadal and sub-decadal time-scales, a better understanding is needed of the aspects of mode water that may be important for biological production.

One likely link is a shifting distribution in open-ocean overwintering stocks, which is expected to align with the transition zone between EMW and LSW (Gislason and Astthorsson, 2000; Heath et al., 2000), and thus the subarctic front. When the front is shifted toward Iceland, the advection path to the shelf is shorter, and more direct, increasing the *Front-to-shelf flows* (2). Such frontal shifts occur on sub-decadal time scales, primarily driven by regional *air-sea heat exchanges* and *wind stress curls* (Eden and Willebrand, 2001), and northward shifts that generally follow an increase to a high NAO, after a time-lag of 1–2 years (Thierry et al., 2008).

The flow field itself might also change in relation to the mode water dynamics. On-shelf flux is most direct from the Iceland Basin, but a contribution from the NE Irminger Sea is not unrealistic, although it would oppose the generally accepted flow scheme (Valdimarsson and Malmberg, 1999). Deep isopycnal flows are dominated by cyclonic paths south of Iceland (Bower et al., 2002), but the near-surface (Brambilla and Talley, 2008a; Reverdin et al., 2003) and the near-slope flows (Logemann et al., 2013) are more northeastward directed. After ascent, *C. finmarchicus* congregates in a wind influenced stratified near-surface layer and the *Front-to-shelf flows* (2) from the Irminger Sea can be considerable (Fig. 5). The general flows in the Reykjanes Ridge region are also more northeastward directed toward Iceland during NAO-high condition (Flatau et al., 2003), which likewise is likely to enhance the *Front-to-shelf flows*.

Processes impacting the size of the overwintering stocks must also be important, and temperature is typically considered, when attempting to link biological changes to the environment (e.g. Richardson and Schoeman, 2004; Stenseth et al., 2002). The hydrography of the mode waters varies relatively modestly, with much energy on decadal to multi-decadal time scales (Hátún et al., 2005). We thus find it unlikely that hydrographic changes *per se* induce the observed zooplankton variability.

Deep mixed layer depths (MLD) are, on the other hand, expected to enhance biological production in several ways. Several hypothesis have recently been proposed, to explain the significant depth-integrated primary production, prior to the onset of the classical spring bloom (Chiswell et al., 2015) explained by the critical-depth hypothesis (Sverdrup, 1953). The *phyto-convection* hypothesis (Backhaus et al., 1999) says that vertical motion enables remixing of diatoms from suspended deep populations, and thus seeds the spring bloom with this fast-growing algal species (Smetacek, 1985), which is also observed in the subpolar Atlantic (Daniels et al., 2015). The *disturbance-recovery* hypothesis (Behrenfeld, 2010) suggests that blooms are triggered by a reduction in phytoplankton losses (grazing) during deep winter mixing, while the *critical-turbulence* hypothesis suggests that low vertical mixing after terminated convective overturn allows phytoplankton to stratify within a deep mixed layer (Huisman et al., 1999; Taylor and Ferrari, 2011). This early deep bloom might increase the food availability for *C. finmarchicus* during their ascent phase toward the surface during March–April (Gislason and Astthorsson, 2000). Convection is also mixing up nutrients from the nutrient rich waters below (Ólafsson, 2003), which might postpone nutrient limitation during the summer production period (Henson et al., 2006).

The formation of mode waters likewise depends on the time variability of the MLD and the horizontal transport through the mixed layer (Brambilla et al., 2008b). The variability of the MLD is primarily driven by air-sea heat (buoyancy) exchange, and the spatial scales in the atmosphere are large. A strong winter will lead to increased heat losses all along the main storm track, from the Labrador Sea, across the Irminger and Iceland basins and into the Nordic Seas. Deeper MLD are therefore occurring concurrently in the NW Iceland Basin (EMW) and the Irminger Sea (WMW) (Fig. 8). Supporting a possible link to MLD variability, we show high correlations between the *MLD in the NIS* (5), and both the *On-shelf zooplankton* (1) and the CPR-derived *SPG C. finmarchicus abundance* (4), respectively (Fig. 9). The annual averaged CPR record that we have utilized is dominated by the number of adult animals (stages C5 and C6) during summer (June and July). The correlation with MLD indicates that productive oceanic conditions are beneficial for the first new generation of *C. finmarchicus*, both within the subpolar gyre and on the south Iceland shelf.

The 'high-or-low' variability is more pronounced in the MLD series than in the gyre index (cf. Figs. 6c and 9). We therefore postulate that vertical convective processes are more important for the production of *C. finmarchicus*, than are the slower large-scale advective processes associated with the variable admixture of waters from the subtropical gyre and the SPG.

Because of the possible importance of the NIS, in addition to the NW Iceland Basin, and the potential for prediction in the Irminger Sea (see below), we focus subsequently on processes in the Labrador-Irminger Sea (WMW).

Shorter term variability is particularly clear in the Labrador Sea, where the average production rate of LSW is only about 1.5 Sv ($1\ Sv = 10^6\ m^3\ s^{-1}$), except for peaks reaching 7–12 Sv when convection is deep (Deshayes et al., 2007). The closest correlations between the air-sea heat exchanges and the *MLD in the NIS* (5) are also identified in the Labrador Sea, just south of Greenland (Fig. 10a).

A winter with strong *Air-sea heat exchange* at year y_0 will make the water column denser (Fig. 10) and induce deep convection in the Labrador-south Irminger Seas. Under the action of gravity, these anomalously dense WMW will slide isopycnally northeastward toward the Reykjanes Ridge in the *Lab Sea-to-front flows* (8), where they will precondition the water column during the subsequent winter ($y_0 + 1$ yr) (Fig. 12b). This pre-conditioning renders 'memory' to the system, so that even with weaker *air-sea heat exchanges* during the following winter, deep convection might still take place within the Irminger Sea (de Jong et al., 2012; Pickart et al., 2003). The *Lab Sea-to-front flows* might also transport zooplankton from the center of abundance in the western SPG, but we find that the advection of physical properties (weakly stratified WMW) is probably more important than the influx of animals.

In addition to the impact on stratification in the NIS, increased volumes of WMW, reinforced by *Wind stress curl* (Ekman pumping), induce lifting of the isopycnals, and are therefore likely, after a time lag, to shift *the Frontal position* in the NE Irminger Sea.

Our results thus hold promise for ocean and ecosystem operational intra-seasonal predictions (late winter to summer), and maybe even with some skill the following year due to the lagged preconditioning effect of WMW. An attempt to develop a predictive tool has been carried out by the US National Multi-Model Ensemble (NMME) seasonal climate forecasting system (Kirtman et al., 2014). Retrospective forecast (1982–2010) skill maps of

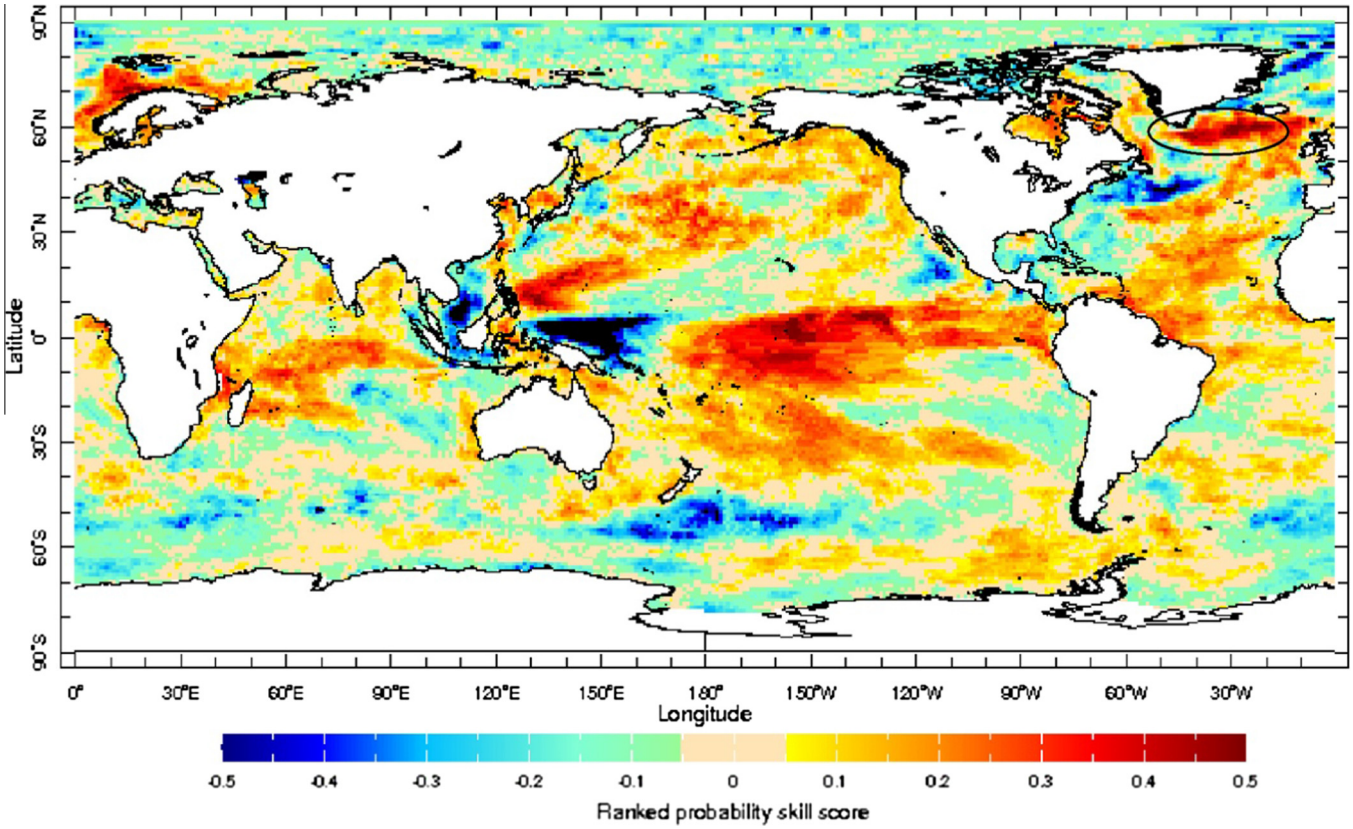

Fig. 13. The Ranked Probability Skill Score (Weigel et al., 2007) of sea surface temperature (SST), from a retrospective forecast analysis (1982–2010) performed by the US National Multi-Model Ensemble (NMME) seasonal forecasting system (http://www.cpc.ncep.noaa.gov/products/NMME/). The predictive skill of hindcasts initiated during March in forecasting the SST variations of the subsequent winter (December to February) is shown. The study region is emphasized with a black oval.

SST show that our study region (the Irminger Sea and Reykjanes Ridge) is, together with the central tropical Pacific, the most predictable region in the World oceans on intra-seasonal to inter-annual time scales. This is illustrated here through the predictive skill of hindcasts initiated during March to forecast SST in the subsequent winter (December–February) (Fig. 13, the International Research Institute for Climate and Society forecast evaluation online tool at http://iridl.ldeo.columbia.edu/SOURCES/.Models/.NMME/).

Winter-spring SST is closely related to the density of the deep mixed layer, and thus to the MLD. The mechanism underlying the potential SST predictability here is likely associated with, and thus representative of, the advective process from the Labrador Sea to the NIS region (Figs. 4 and 7).

We suggest that the much discussed 'cold blob' south of Greenland in 2015 is not linked to a weakened Atlantic Meridional Overturning Circulation as suggested by Rahmstorf et al. (2015), but merely to enhanced winter cooling, and thus convection in the Labrador-Irminger Seas during the two winters between 2013 and 2015. According to our finding, this should have led to increased biological productivity on the shelves adjacent to the SPG during the production seasons in 2014 and/or 2015.

6. Conclusions

Based on a comprehensive analysis of observed and simulated atmospheric and oceanic spatio-temporal datasets, together with principal biological observations, we have identified key atmospheric and oceanic drivers behind the marked sub-decadal zooplankton variability in the northwestern Atlantic. The main conclusions are: (*i*) The abundance of *C. finmarchicus* within the subpolar gyre and on the south Iceland shelf may be regulated by the mode water dynamics in the Labrador-Irminger and Iceland Basins, (*ii*) convective processes, proxied by the winter mixed layer depths, amplify the characteristic 'high-or-low' states of this system and (*iii*) remote forcing from the Labrador Sea might provide a 0.5–1.5 year predictability horizon.

Acknowledgements

The research leading to these results has received funding from the European Union 7th Framework Programme (FP7 2007–2013), under grant agreement no. 308299 NACLIM www.naclim.eu.

HH was partly funded through the Danish project NAACOS 10-093903/DSF.

DM was supported by the Federal Ministry for Education and Research (BMBF) RACE project (FKZ: 03F0729D). S.P. was funded by the Danish government through the program 'Marine Climate in the North Atlantic and its Effects on Plankton and Fish'. Support was also provided by the Nordic Council of Ministers (AEG-11323).

The model simulation was conducted at the German Climate Computing Center (DKRZ). The altimeter products were produced by Ssalto/Duacs and distributed by Aviso (http://www.jason.oceanobs.com/html/donnees/duacs/welcome_uk.html), with support from CNES.

Appendix A

A.1. Lagged correlations

The *On-shelf zooplankton* peaks sampled during May are time-lagged relative to the winter integrated physical records.

The zooplankton peaks occur the same summer, and or the following summer (at most 1.5 years after the physical driver). It is not strictly meaningful to lag-correlated annual records, but to give an estimate of this important average time-lag, annually averaged time series are interpolated onto monthly values (linearly), and then shifted by monthly increments until maximum correlation coefficients between the physical forcing and the zooplankton record is obtained (Table 1 and in text). The correlation coefficients are calculated by a standard Matlab routine which does not account for autocorrelation. The *p*-values are computed by transforming the correlation to create a *t*-statistic having $N-2$ degrees of freedom, where N is the sample size. High-passed time series (calculated by subtracting low-passed series using a six years wide Boxcar filter) are also tested in order to emphasize valuable synchronies, which often ride on longer term trends (Table 1).

A.2. Front-to-shelf flows

In the particle tracking experiments we use daily flow fields from the MPI-OM simulation, interpolated on a regular ($0.25° \times 0.25°$) grid. Near the subarctic front, *C. finmarchicus* ascends to the surface layer in March–May, with the most rapid increase in near-surface abundances during April (Fig. 2a and b). 'Particles' are therefore seeded in the surface layer, once a week through April during the period 1970–2010. This is done within a triangle covering the Reykjanes Ridge east and west from the summit to the 2000 m isobath. The seeding region covers the latitudes 60–63.75°N, with the northernmost edge covering longitudes 20–27.5°W and the southernmost edge 28–29.75°W (Figs. 10 and A.1a, Section 4.1). The target location for the particles is a circle with a radius of 100 km at the southwestern Iceland shelf edge at Selvogsgrunn (centered at 63.25°N, 21.5°W) (Figs. 5 and A.1a)

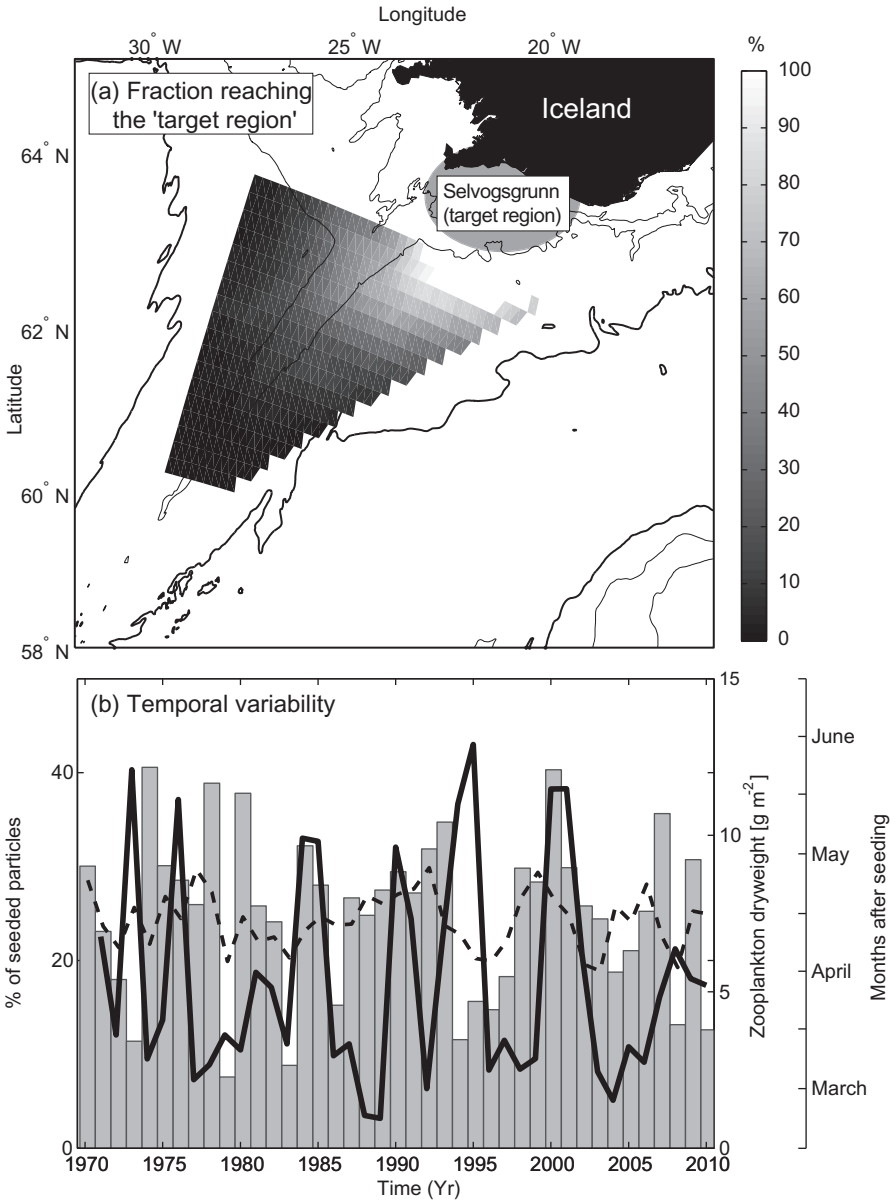

Fig. A.1. (a) The fraction of all particles seeded within the shown triangle during April, which pass through the near-shelf target region (shaded circle), before mid-June. (b). Temporal variability of the horizontal transport. The bars show the percentage of particles seeded within the seeding region that reached the target region shown in (a) (left axis). The average drift time for each year, and the *on-shelf zooplankton* record are shown with dashed and bold black lines, respectively (right axes). Note that the percentages appear too low, since many particles from the south-western part of the seeding region do not reach the target region within the short duration (April–June).

Table A1
The selected metrics and their inter-linkages.

Metric	Determines potentially	Potentially determined by	Calculated as
(1) On-shelf zooplankton	Higher trophic levels on the shelf	*SPG C. finmarchicus abundances (4)* *Front-to-shelf flows* (2) *Frontal position* (3)	On-shelf observations during May (Sections 2.3 and 3)
(2) Front-to-shelf flows (near-surface)	The transport of zooplankton (and nutrients) from the source region toward the shelf *On-shelf zooplankton* (1)	The *Frontal position* (3) Local *Wind stress (curl)* (7) Summer stratification	Particle tracking using simulated flow fields (Section 4.1)
(3) Frontal position	The distance from the source region to the shelf The *Front-to-shelf flows* (2) *On-shelf zooplankton* (1)	Convection in the Labrador-south Irminger Seas *Lab Sea-to-front flows* (8) *Wind stress curl* (7)	EOF analysis of simulated (MPI-OM) sea surface height field (Section 4.2)
(4) *SPG C. finmarchicus abundances*	Abundance of source zooplankton in the Frontal zone Northward transport of zooplankton from the SPG toward the Frontal zone *On-shelf zooplankton* (1)	*MLD in the NIS (5)* (and the processes potentially determined by convection) Convection in the Labrador-south Irminger Seas	Averaged CPR data (Mar–Oct) of *C. finmarchicus*, stages C5 and C6 (Section 4.3).
(5) MLD in the NIS	Pre-bloom nutrient concentrations The pre-bloom primary production through e.g. the 'phyto-convection' mechanism The post-bloom primary production through nutrient limitation *SPG C. finmarchicus abundances (4)*	Local *Air-sea heat exchange* (6) Local *Wind stress curl* (7) Convection in the Labrador-south Irminger Seas *Lab Sea-to-front flows* (8)	Taken from the simulations in the northern Irminger Sea during March (Section 4.3).
(6) Air-sea heat exchange	MLD in the NIS (5) Convection in the Labrador-south Irminger Seas *Lab Sea-to-front flows* (8)	NAO-related large-scale atmospheric dynamics	NCAR/NCEP reanalysis fields of latent, sensible and radiative fluxes (Section 4.4).
(7) Wind stress curl	*MLD* in the NIS (5) *Frontal position* (3) The general flow field (2,8)	NAO-related large-scale atmospheric dynamics	NCAR/NCEP reanalysis fields of momentum fluxes (Section 4.4).
(8) Lab Sea-to-front flows	Pre-conditioning and thus *MLD in the NIS* (5) The *Frontal position* (3) Influx of zooplankton from center of abundance in south	Convection in the Labrador-south Irminger Seas	Particle tracking using simulated flow fields (Section 4.5.2).

Table A2
Details of the particle tracking experiments.

Seeding date	Tracking length	Target date	Seeding region	Target region	Nr. of particles
Toward front					
1st of March Yearly	3 years		Southern Irminger Sea 55.25–57.75°N 40–44°W	Circle (r = 100 km) centered at 63°N, 32°W	1066 (per seeding)
Toward shelf					
April, Weekly	0.5–3.5 months	15th of June	Triangular region covering the Reykjanes Ridge east and west from the summit to the 2000 m isobath. Between the latitudes 60–63.75°N. The northern edge spans the longitude 20–27.5°W and the southern edge 28–29.75°W	Circle (r = 100 km) centered at 63.25°N, 21.5°W	462 (per seeding) 6468 (per year)

and a tracking time that ends in mid-June (Table A2), when the *On-shelf zooplankton* observations were made.

A.3. Lab Sea-to-front flows

The *Lab Sea-to-front flows* (8) (Fig. 4, Table A1) experiment examines preconditioning of convection in the NIS by the unstable (WMW). Particles are seeded in the southern Irminger Sea in the depth layer at 420 m in a grid box covering 55.25–57.75°N, 40–44°W (Fig. 12a). Particles are seeded on the first of March every year during the period 1970–2007 and tracked for three years (Table A2). A 'target area' is defined as a circle in the NIS with radius of 100 km and center at 63°N, 32°W. We analyze drift time and number of particles that reach the designated target area (Fig. 12, Section 4.5.2).

References

Alheit, J., Licandro, P., Coombs, S., Garcia, A., Giraldez, A., Santamaria, M.T.G., Slotte, A., Tsikliras, A.C., 2014. Atlantic Multidecadal Oscillation (AMO) modulates dynamics of small pelagic fishes and ecosystem regime shifts in the eastern North and Central Atlantic. Journal of Marine Systems 131, 21–35.

Alheit, J., Pohlmann, T., Casini, M., Greve, W., Hinrichs, R., Mathis, M., O'Driscoll, K., Vorberg, R., Wagner, C., 2012. Climate variability drives anchovies and sardines into the North and Baltic Seas. Progress in Oceanography 96, 128–139.

Astthorsson, O.S., Gislason, A., 1995. Long-term changes in zooplankton biomass in Icelandic waters in spring. ICES Journal of Marine Science 52, 657–668.

Astthorsson, O.S., Hallgrimsson, I., Jonsson, S., 1983. Variations in zooplankton densities in Icelandic waters in spring during the years 1961–1982. Rit Fiskideildar 7, 73–113.

Backhaus, J.O., Hegseth, E.N., Wehde, H., Irigoien, X., Hatten, K., Logemann, K., 2003. Convection and primary production in winter. Marine Ecology Progress Series 251, 1–14.

Backhaus, J.O., Wehde, H., Hegseth, E.N., Kampf, J., 1999. 'Phyto-convection': the role of oceanic convection in primary production. Marine Ecology Progress Series 189, 77–92.

Bainbridge, V., McKay, B.J., 1968. The Feeding of Cod and Redfish Larvae. International Commission for the Northwest Atlantic Fisheries Special Publication No. 7, pp. 187–217.
Batten, S.D., Clark, R., Flinkman, J., Hays, G., John, E., John, A.W.G., Jonas, T., Lindley, J. A., Stevens, D.P., Walne, A., 2003. CPR sampling: the technical background, materials and methods, consistency and comparability. Progress in Oceanography 58, 193–215.
Behrenfeld, M.J., 2010. Abandoning Sverdrup's critical depth hypothesis on phytoplankton blooms. Ecology 91, 977–989.
Belkin, I.M., 2004. Propagation of the "Great Salinity Anomaly" of the 1990s around the northern North Atlantic. Geophysical Research Letters 31. http://dx.doi.org/10.1029/2003GL019334.
Bersch, M., Meincke, J., Sy, A., 1999. Interannual thermohaline changes in the northern North Atlantic 1991–1996. Deep-Sea Research Part II-Topical Studies in Oceanography 46, 55–75.
Bersch, M., Yashayaev, I., Koltermann, K.P., 2007. Recent changes of the thermohaline circulation in the subpolar North Atlantic. Ocean Dynamics 57, 223–235.
Bleck, R., Rooth, C., Hu, D.M., Smith, L.T., 1992. Salinity-driven thermocline transients in a wind-forced and thermohaline-forced isopycnic coordinate model of the North-Atlantic. Journal of Physical Oceanography 22, 1486–1505.
Bower, A.S., Le Cann, B., Rossby, T., Zenk, W., Gould, J., Speer, K., Richardson, P.L., Prater, M.D., Zhang, H.M., 2002. Directly measured mid-depth circulation in the northeastern North Atlantic Ocean. Nature 419, 603–607.
Boyer, T.P., Antonov, J.I., Garcia, H.E., Johnson, D.R., Locarnini, R.A., Mishonov, A.V., Pitcher, M.T., Baranova, O., Smolyar, I., Levitus, S., 2006. World Ocean Database 2005. NOAA Atlas NESDIS 60.
Brambilla, E., Talley, L.D., 2008a. Subpolar Mode Water in the northeastern Atlantic: 1. Averaged properties and mean circulation. J. Geophys. Res.-Oceans 113. http://dx.doi.org/10.1029/2006JC004062.
Brambilla, E., Talley, L.D., Robbins, P.E., 2008b. Subpolar Mode Water in the northeastern Atlantic: 2. Origin and transformation. J. Geophys. Res.-Oceans 113. http://dx.doi.org/10.1029/2006JC004063.
Chiswell, S.M., Calil, P.H.R., Boyd, P.W., 2015. Spring blooms and annual cycles of phytoplankton: a unified perspective. Journal of Plankton Research 37, 500–508.
Curry, R.G., 2002. HydroBase 2: A Database of Hydrographic Profiles and Tools for Climatological Analysis, vol. 81. Woods Hole Oceanographic Institution, 96-01.
Daniels, C.J., Poulton, A.J., Esposito, M., Paulsen, M.L., Bellerby, R., St. John, M., Martin, A.P., 2015. Phytoplankton dynamics in contrasting early stage North Atlantic spring blooms: composition, succession, and potential drivers. Biogeosciences 12, 2395–2409.
de Jong, M.F., Van Aken, H.M., Våge, K., Pickart, R.S., 2012. Convective mixing in the central Irminger Sea: 2002–2010. Deep-Sea Research Part I-Oceanographic Research Papers 63, 36–51.
Deshayes, J., Frankignoul, C., Drange, H., 2007. Formation and export of deep water in the Labrador and Irminger Seas in a GCM. Deep-Sea Research Part I-Oceanographic Research Papers 54, 510–532.
Despres, A., Reverdin, G., d'Ovidio, F., 2011. Mechanisms and spatial variability of meso scale frontogenesis in the northwestern subpolar gyre. Ocean Modelling 39, 97–113.
Dickson, R.R., Meincke, J., Malmberg, S.A., Lee, A.J., 1988. The great salinity anomaly in the Northern North-Atlantic 1968–1982. Progress in Oceanography 20, 103–151.
Drinkwater, K., Belgrano, A., Borja, A., Conversi, A., Edwards, M., Greene, C.H., Ottera, O.H., Pershing, A.J., Walker, H., 2003. The response of marine ecosystems to climate variability associated with the North Atlantic Oscillation. In: Hurrell, J. W., Kushnir, Y., Ottera, O.H., Visbeck, M. (Eds.), The North Atlantic Oscillation: Climatic Significance and Environmental Impact. pp. 211–234.
Drinkwater, K., Colbourne, E., Loeng, H., Sundby, S., Kristiansen, T., 2013. Comparison of the atmospheric forcing and oceanographic responses between the Labrador Sea and the Norwegian and Barents seas. Progress in Oceanography 114, 11–25.
Eden, C., Willebrand, J., 2001. Mechanism of interannual to decadal variability of the North Atlantic circulation. Journal of Climate 14, 2266–2280.
Egge, J.K., Aksnes, D.L., 1992. Silicate as regulating nutrient in phytoplankton competition. Marine Ecology-Progress Series 83, 281–289.
Flatau, M.K., Talley, L., Niiler, P.P., 2003. The North Atlantic Oscillation, surface current velocities, and SST changes in the subpolar North Atlantic. Journal of Climate 16, 2355–2369.
Folkow, L.P., Blix, A.S., 1999. Diving behaviour of hooded seals (*Cystophora cristata*) in the Greenland and Norwegian Seas. Polar Biology 22, 61–74.
Folkow, L.P., Martensson, P.E., Blix, A.S., 1996. Annual distribution of hooded seals (*Cystophora cristata*) in the Greenland and Norwegian Seas. Polar Biology 16, 179–189.
Frederiksen, M., Edwards, M., Mavor, R., Wanless, S., 2007. Regional and annual variation in black-legged kittiwake breeding productivity is related to sea surface temperature. Marine Ecology-Progress Series 350, 137–143.
Frederiksen, M., Moe, B., Daunt, F., Phillips, R.A., Barrett, R.T., Bogdanova, M.I., Boulinier, T., Chardine, J.W., Chastel, O., Chivers, L.S., Christensen-Dalsgaard, S., Clement-Chastel, C., Colhoun, K., Freeman, R., Gaston, A.J., Gonzalez-Solis, J., Goutte, A., Gremillet, D., Guilford, T., Jensen, G.H., Krasnov, Y., Lorentsen, S.H., Mallory, M.L., Newell, M., Olsen, B., Shaw, D., Steen, H., Strom, H., Systad, G.H., Thorarinsson, T.L., Anker-Nilssen, T., 2011. Multicolony tracking reveals the winter distribution of a pelagic seabird on an ocean basin scale. Diversity and Distributions 18, 530–542.
Gaard, E., Hansen, B., Olsen, B., Reinert, J., 2002. Ecological features and recent trends in the physical environment, plankton, fish stocks, and seabirds in the Faroe Shelf ecosystem. In: Sherman, K., Skjoldal, H.R. (Eds.), Large Marine Ecosystems of the North Atlantic. Elsevier Science, pp. 245–265.
Garcia H.E., Locarnini, R.A., Boyer, T.P., Antonov, J.I. 2010. World Ocean Atlas 2009, Volume 4: Nutrients (Phosphate, Nitrate, Silicate). U.S. Government Printing Office, Washington, D.C., p. 26.
Gislason, A., Astthorsson, O.S., 2000. Winter distribution, ontogenetic migration, and rates of egg production of *Calanus finmarchicus* southwest of Iceland. ICES Journal of Marine Science 57, 1727–1739.
Gislason, A., Astthorsson, O.S., Petursdottir, H., Gudfinnsson, H., Bodvarsdottir, A.R., 2000. Life cycle of *Calanus finmarchicus* south of Iceland in relation to hydrography and chlorophyll a. ICES Journal of Marine Science 57, 1619–1627.
Gislason, A., Petursdottir, H., Astthorsson, O.S., Gudmundsson, K., Valdimarsson, H., 2009. Inter-annual variability in abundance and community structure of zooplankton south and north of Iceland in relation to environmental conditions in spring 1990–2007. Journal of Plankton Research 31, 541–551.
Gislason, A., Petursdottir, H., Gudmundsson, K., 2014. Long-term changes in abundance of *Calanus finmarchicus* south and north of Iceland in relation to environmental conditions and regional diversity in spring 1990–2013. ICES Journal of Marine Science 71, 2539–2549.
Greene, C.H., Pershing, A.J., 2000. The response of *Calanus finmarchicus* populations to climate variability in the Northwest Atlantic: basin-scale forcing associated with the North Atlantic Oscillation. ICES Journal of Marine Science 57, 1536–1544.
Gudfinnsson, H., Debes, H., Falkenhaug, T., Gaard, E., Gislason, A., Petursdottir, H., Valdimarsson, H., Sigurdsson, T., Stupnikova, A., 2014. Abundance and productivity of the pelagic ecosystem across the northern Mid-Atlantic Ridge in June 2003. ICES CM C12.
Häkkinen, S., Rhines, P.B., 2004. Decline of subpolar North Atlantic circulation during the 1990s. Science 304, 555–559.
Harms, J.H., Heath, M.R., Bryant, A.D., Backhaus, J.O., Hainbucher, D.A., 2000. Modelling the Northeast Atlantic circulation: implications for the spring invasion of shelf regions by *Calanus finmarchicus*. ICES Journal of Marine Science 57, 1694–1707.
Hátún, H., Jacobsen, J.A., Sandø, A.B., 2007. Environmental influence on the spawning distribution and migration pattern of northern blue whiting (*Micromesistius poutassou*). ICES CM 2007/B06, 14p.
Hátún, H., McClimans, T.A., 2003. Monitoring the Faroe Current using altimetry and coastal sea-level data. Continental Shelf Research 23, 859–868.
Hátún, H., Payne, M., Beaugrand, G., Reid, P.C., Sandø, A.B., Drange, H., Hansen, B., Jacobsen, J.A., Bloch, D., 2009a. Large bio-geographical shifts in the north-eastern Atlantic Ocean: from the subpolar gyre, via plankton, to blue whiting and pilot whales. Progress in Oceanography 80, 149–162.
Hátún, H., Payne, M.R., Jacobsen, J.A., 2009b. The North Atlantic subpolar gyre regulates the spawning distribution of blue whiting (*Micromesistius poutassou*). Canadian Journal of Fisheries and Aquatic Sciences 66, 759–770.
Hátún, H., Sandø, A.B., Drange, H., Hansen, B., Valdimarsson, H., 2005. Influence of the Atlantic subpolar gyre on the thermohaline circulation. Science 309, 1841–1844.
Heath, M.R., Fraser, J.G., Gislason, A., Hay, S.J., Jonasdottir, S.H., Richardson, K., 2000. Winter distribution of *Calanus finmarchicus* in the Northeast Atlantic. ICES Journal of Marine Science 57, 1628–1635.
Heath, M.R., Rasmussen, J., Ahmed, Y., Allen, J., Anderson, C.I.H., Brierley, A.S., Brown, L., Bunker, A., Cook, K., Davidson, R., Fielding, S., Gurney, W.S.C., Harris, R., Hay, S., Henson, S., Hirst, A.G., Holliday, N.P., Ingvarsdottir, A., Irigoien, X., Lindeque, P., Mayor, D.J., Montagnes, D., Moffat, C., Pollard, R., Richards, S., Saunders, R.A., Sidey, J., Smerdon, G., Speirs, D., Walsham, P., Waniek, J., Webster, L., Wilson, D., 2008. Spatial demography of *Calanus finmarchicus* in the Irminger Sea. Progress in Oceanography 76, 39–88.
Henson, S.A., Sanders, R., Holeton, C., Allen, J.T., 2006. Timing of nutrient depletion, diatom dominance and a lower-boundary estimate of export production for Irminger Basin, North Atlantic. Marine Ecology-Progress Series 313, 73–84.
Heywood, K.J., Mcdonagh, E.L., White, M.A., 1994. Eddy kinetic-energy of the North-Atlantic subpolar gyre from satellite altimetry. Journal of Geophysical Research-Oceans 99, 22525–22539.
Holliday, N.P., Hughes, S.L., Bacon, S., Beszczynska-Moller, A., Hansen, B., Lavin, A., Loeng, H., Mork, K.A., Osterhus, S., Sherwin, T., Walczowski, W., 2008. Reversal of the 1960s–1990s freshening trend in the northeast North Atlantic and Nordic Seas. Geophysical Research Letters 35. http://dx.doi.org/10.1029/2007GL032675.
Hovland, E.K., Dierssen, H.M., Ferreira, A.S., Johnsen, G., 2013. Dynamics regulating major trends in Barents Sea temperatures and subsequent effect on remotely sensed particulate inorganic carbon. Marine Ecology Progress Series 484, 17–32.
Huisman, J., van Oostveen, P., Weissing, F.J., 1999. Critical depth and critical turbulence: two different mechanisms for the development of phytoplankton blooms. Limnology and Oceanography 44, 1781–1787.
Jungclaus, J.H., Fischer, N., Haak, H., Lohmann, K., Marotzke, J., Matei, D., Mikolajewicz, U., Notz, D., von Storch, J.S., 2013. Characteristics of the ocean simulations in the Max Planck Institute Ocean Model (MPI-OM) the ocean component of the MPI-Earth system model. Journal of Advances in Modeling Earth Systems 5, 422–446.
Kalnay, E., Kanamitsu, M., Kistler, R., Collins, W., Deaven, D., Gandin, L., Iredell, M., Saha, S., White, G., Woollen, J., Zhu, Y., Chelliah, M., Ebisuzaki, W., Higgins, W., Janowiak, J., Mo, K.C., Ropelewski, C., Wang, J., Leetmaa, A., Reynolds, R., Jenne, R., Joseph, D., 1996. The NCEP/NCAR 40-year reanalysis project. Bulletin of the American Meteorological Society 77, 437–471.

Kirtman, B.P., Min, D., Infanti, J.M., Kinter, J.L., Paolino, D.A., Zhang, Q., van den Dool, H., Saha, S., Mendez, M.P., Becker, E., Peng, P.T., Tripp, P., Huang, J., Dewitt, D.G., Tippett, M.K., Barnston, A.G., Li, S.H., Rosati, A., Schubert, S.D., Rienecker, M., Suarez, M., Li, Z.E., Marshak, J., Lim, Y.K., Tribbia, J., Pegion, K., Merryfield, W.J., Denis, B., Wood, E.F., 2014. The North American multimodel ensemble phase-1 seasonal-to-interannual prediction; phase-2 toward developing intraseasonal prediction. Bulletin of the American Meteorological Society 95, 585–601.

Lam, N.S.N., 1983. Spatial interpolation methods - a review. American Cartographer 10, 129–149.

Larsen, K.M.H., Hátún, H., Hansen, B., Kristiansen, R., 2012. Atlantic water in the Faroe area: sources and variability. ICES Journal of Marine Science 69, 802–808.

Levitus, S., 1998. Introduction. World Ocean Database 1998, vol. I. 18, 42.

Logemann, K., Olafsson, J., Snorrason, A., Valdimarsson, H., Marteinsdottir, G., 2013. The circulation of Icelandic waters - a modelling study. Ocean Science 9, 931–955.

Marshall, J., Kushner, Y., Battisti, D., Chang, P., Czaja, A., Dickson, R., Hurrell, J., McCartney, M., Saravanan, R., Visbeck, M., 2001. North Atlantic climate variability: phenomena, impacts and mechanisms. International Journal of Climatology 21, 1863–1898.

Marsland, S.J., Haak, H., Jungclaus, J.H., Latif, M., Roske, F., 2003. The Max-Planck-Institute global ocean/sea ice model with orthogonal curvilinear coordinates. Ocean Modelling 5, 91–127.

Matei, D., Baehr, J., Jungclaus, J.H., Haak, H., Muller, W.A., Marotzke, J., 2012a. Multiyear prediction of monthly mean Atlantic meridional overturning circulation at 26.5°N. Science 335, 76–79.

Matei, D., Pohlmann, H., Jungclaus, J., Muller, W., Haak, H., Marotzke, J., 2012b. Two tales of initializing decadal climate prediction experiments with the ECHAM5/MPI-OM model. Journal of Climate 25, 8502–8523.

Matthews, J.B.L., Heimdal, B.R., 1980. Pelagic productivity and food chains in fjord systems. In: Freeland, H.J., Levings, C.D. (Eds.), Fjord Oceanography. Plenum Press, New York, pp. 377–398.

McCartney, M.S., Talley, L.D., 1982. The sub-polar mode water of the North-Atlantic Ocean. Journal of Physical Oceanography 12, 1169–1188.

Meyer-Harms, B., Irigoien, X., Head, R., Harris, R., 1999. Selective feeding on natural phytoplankton by *Calanus finmarchicus* before, during, and after the 1997 spring bloom in the Norwegian Sea. Limnology and Oceanography 44, 154–165.

Muller, W.A., Matei, D., Bersch, M., Jungclaus, J.H., Haak, H., Lohmann, K., Compo, G. P., Sardeshmukh, P.D., Marotzke, J., 2015. A twentieth-century reanalysis forced ocean model to reconstruct the North Atlantic climate variation during the 1920s. Climate Dynamics 44, 1935–1955.

Nejstgaard, J.C., Gismervik, I., Solberg, P.T., 1997. Feeding and reproduction by *Calanus finmarchicus*, and microzooplankton grazing during mesocosm blooms of diatoms and the coccolithophore *Emiliania huxleyi*. Marine Ecology Progress Series 147, 197–217.

Nunez-Riboni, I., Bersch, M., Haak, H., Jungclaus, J.H., Lohmann, K., 2012. A multi-decadal meridional displacement of the Subpolar Front in the Newfoundland Basin. Ocean Science 8, 91–102.

Nye, J.A., Baker, M.R., Bell, R., Kenny, A., Kilbourne, K.H., Friedland, K.D., Martino, E., Stachura, M.M., Van Houtan, K.S., Wood, R., 2014. Ecosystem effects of the Atlantic multidecadal oscillation. Journal of Marine Systems 133, 103–116.

Ólafsson, J., 2003. Winter mixed layer nutrients in the Irminger and Iceland Seas, 1990–2000. ICES Marines Science Symposia 219, 329–332.

Pedchenko, A.P., 2005. The role of interannual environmental variations in the geographic range of spawning and feeding concentrations of redfish *Sebastes mentella* in the Irminger Sea. ICES Journal of Marine Science 62, 1501–1510.

Pickart, R.S., Spall, M.A., Ribergaard, M.H., Moore, G.W.K., Milliff, R.F., 2003. Deep convection in the Irminger Sea forced by the Greenland tip jet. Nature 424, 152–156.

Postel, L., Fock, K., Hagen, W., 2000. Biomass and abundance. In: Harris, R., Wiebe, P., Lenz, J., Skjoldal, H.R., Huntley, M. (Eds.), ICES Zooplankton Methodology Manual. Academic Press, New York, pp. 83–192.

Rahmstorf, S., Box, J.E., Feulner, G., Mann, M.E., Robinson, A., Rutherford, S., Schaffernicht, E.J., 2015. Exceptional twentieth-century slowdown in Atlantic Ocean overturning circulation. Nature Climate Change 5, 475–480.

Reverdin, G., Niiler, P.P., Valdimarsson, H., 2003. North Atlantic Ocean surface currents. Journal of Geophysical Research-Oceans 108. http://dx.doi.org/10.1029/2001JC001020.

Richardson, A.J., Schoeman, D.S., 2004. Climate impact on plankton ecosystems in the Northeast Atlantic. Science 305, 1609–1612.

Richter, K., Segtnan, O.H., Furevik, T., 2012. Variability of the Atlantic inflow to the Nordic Seas and its causes inferred from observations of sea surface height. Journal of Geophysical Research-Oceans, 117.

Robson, J., Sutton, R., Lohmann, K., Smith, D., Palmer, M.D., 2012. Causes of the rapid warming of the North Atlantic Ocean in the mid-1990s. Journal of Climate 25, 4116–4134.

Sanders, R., Brown, L., Henson, S., Lucas, M., 2005. New production in the Irminger Basin during 2002. Journal of Marine Systems 55, 291–310.

Sandø, A.B., Furevik, T., 2008. Relation between the wind stress curl in the North Atlantic and the Atlantic inflow to the Nordic Seas. Journal of Geophysical Research-Oceans 113, C06028. http://dx.doi.org/10.1029/2007JC004236.

Siegismund, F., Johannessen, J., Drange, H., Mork, K.A., Korablev, A., 2007. Steric height variability in the Nordic Seas. Journal of Geophysical Research-Oceans 112. http://dx.doi.org/10.1029/2007JC004221.

Silva, T., Gislason, A., Licandro, P., Marteinsdottir, G., Ferreira, A.S., Gudmundsson, K., Astthorsson, O.S., 2014. Long-term changes of euphausiids in shelf and oceanic habitats southwest, south and southeast of Iceland. Journal of Plankton Research, 1–17.

Smetacek, V.S., 1985. Role of sinking in diatom life-history cycles - ecological, evolutionary and geological significance. Marine Biology 84, 239–251.

Solmundsson, J., Jonsson, E., Bjornsson, H., 2010. Phase transition in recruitment and distribution of monkfish (*Lophius piscatorius*) in Icelandic waters. Marine Biology 157, 295–305.

Stefánsson, U., Ólafsson, J., 1991. Nutrients and fertility of Icelandic Waters. Rit Fiskideildar 7, 1–56.

Stenseth, N.C., Mysterud, A., Ottersen, G., Hurrell, J.W., Chan, K.S., Lima, M., 2002. Ecological effects of climate fluctuations. Science 297, 1292–1296.

Sundby, S., 2000. Recruitment of Atlantic cod stocks in relation to temperature and advection of copepod populations. Sarsia 85, 277–298.

Sverdrup, H.U., 1953. On conditions for the vernal blooming of phytoplankton. Journal du Conseil 18, 287–295.

Sy, A., Rhein, M., Lazier, J.R.N., Koltermann, K.P., Meincke, J., Putzka, A., Bersch, M., 1997. Surprisingly rapid spreading of newly formed intermediate waters across the North Atlantic Ocean. Nature 386, 675–679.

Taylor, J.R., Ferrari, R., 2011. Shutdown of turbulent convection as a new criterion for the onset of spring phytoplankton blooms. Limnology and Oceanography 56, 2293–2307.

Thierry, V., de Boisseson, E., Mercier, H., 2008. Interannual variability of the Subpolar Mode Water properties over the Reykjanes Ridge during 1990–2006. Journal of Geophysical Research-Oceans 113. http://dx.doi.org/10.1029/2007JC004443.

Valdimarsson, H., Malmberg, S.A., 1999. Near-surface circulation in Icelandic waters derived from satellite tracked drifters. Rit Fiskideildar, 23–29.

Víkingsson, G.A., Pike, D.G., Desportes, G., Øien, N., Gunnlaugsson, T., Bloch, D., 2009. Distribution and abundance of fin whales (*Balaenoptera physalus*) in the Northeast and Central Atlantic as inferred from the North Atlantic Sightings Surveys 1987–2001. NAMMCO Scientific Publications 7, 49–72.

Weigel, A.P., Liniger, M.A., Appenzeller, C., 2007. The discrete Brier and ranked probability skill score. Monthly Weather Review 135, 118–124.

Yashayaev, I., Bersch, M., Van Aken, H.M., 2007. Spreading of the Labrador Sea Water to the Irminger and Iceland basins. Geophysical Research Letters 34. http://dx.doi.org/10.1029/2006GL028999.